Aerodynamic Analysis and Shape Optimization of Non-axisymmetric Bodies

AE 797 M.Tech. Project Report
by

Manideep Reddy Desham
(Roll No. 163010004)

Supervisor:
Prof. Rajkumar S. Pant

Department of Aerospace Engineering
Indian Institute of Technology Bombay
Mumbai 400076 (India)

18 June 2018

Acceptance Certificate

Department of Aerospace Engineering

Indian Institute of Technology Bombay

The project report entitled "Aerodynamic Analysis and Shape Optimization of Non-axisymmetric Bodies" submitted by Manideep Reddy Desham (Roll No. 163010004) may be accepted for being evaluated.

Date: 18 June 2018

Prof. Rajkumar S. Pant

Abstract

Aerodynamic shape optimization is the process of obtaining the most suitable (preferably low drag) airship envelope shape to a given problem. Multidisciplinary shape optimization means obtaining better shape subject to the trade off between performance parameters of different disciplines.

Most of the existing studies related to shape optimization of airships consider their envelopes to be axisymmetric bodies. However there are many Possibilities for non-axisymmetric envelopes.One example for the case of non-axisymmetric envelope is the case of stratospheric airships, which require an flat upper surface for making provision to mount solar panel as they are mostly powered by the solar power. Low drag shapes are preferred in airships because the power/ fuel consumption is directly dependent on drag coefficient. The drag coefficient of axisymmetric envelopes can be estimated by performing 2D CFD analysis, but non-axisymmetric envelope shapes needs 3D CFD analysis to be performed, which demands more computational effort.

The present study aims at developing a Surrogate Based Design Optimization (SBDO) methodology for obtaining minimum drag shapes which are non-axisymmetric. A novel scheme for geometry parameterization of envelope shapes of a given volume is presented, using modified Gertler Series 58 Shape Generator. Latin Hyper-cube Sampling is used to generate 80 shapes, and the volumetric drag coefficient (C_{DV}) of the envelope is determined at these 80 shapes/ design points by carrying out 3-D CFD analysis using OpenFOAM®. A simple *Kriging* based surrogate model was fitted through these points, which predicted C_{DV} values within 6% accuracy at 8 randomly generated trial shapes. A shape corresponding to minimum C_{DV} of this surrogate function was obtained using Genetic Algorithm (GA) optimizer. It has been found that the optimal shape for minimum drag is found to be an axisymmetric body. However if we give constraint that the body should be non-axisymmetric, the drag increased by 14.92 %.

Table of Contents

List of Figures

List of Tables

Chapter 1

Background and Introduction

Figure 1.1: Airship with non-axisymmetric envelope [24]

Unconventional non-axisymmetric shape provides many advantages over conventional axisymmetric shapes. They can have flatter upper surface and is advantageous for capturing more solar irradiance in the case of stratospheric airships with solar panels on the top. Existing literature has good amount of work done on CFD analysis of axisymmetric shapes but not on non-axisymmetric shapes. The reason is obvious, 2D analysis can easily be done for axisymmetric shapes. But to analyze non-axisymmetric shapes, we need to perform 3D CFD analysis. It demands more computational power which might not be available for many researchers. An open source CFD software called OpenFOAM® (Open source Field Operation And Manipulation) has been used in our present study to perform CFD analysis. OpenFOAM® comes with an inbuilt meshing (*Block mesh* and *Snappy Hex Mesh*) and post-processing (*Paraview*) utilities, both of which are known for their unique and advanced method of problem solving capabilities.

1.1 Objective

The project is divided into two parts. In the first part, OpenFOAM® software is validated using existing CFD results available in the literature for four standard shapes. A framework for carrying out multi-disciplinary shape optimization has been laid out. The framework is then implemented in second part and arrived at an optimal shape with respect to user requirements.

1.2 Report layout

After providing a brief introduction to shape optimization outlining the aims and objectives of this study, Chapter 2 gives the detailed literature survey of various fields required for multi-disciplinary shape optimization. Chapter 3 gives a brief introduction about OpenFOAM and demonstrates the power and advantages of using OpenFOAM®. Mesh generation using *SnappyHexMesh* is discussed in Section 3.1. Section 3.2 validates the OpenFOAM® software with four axisymmetric standard shapes available in literature. Chapter 4 explains the modified Gertler parameter technique used for the parameterization of geometry.

Chapter 5 gives a brief overview of need for the surrogate model in the optimization routine and explains the concept of surrogate model, design of experiments and formulation of different surrogate models. Section 5.5 explains the SBDO technique using Himmelblau test function. It also validates the Genetic algorithm code by Xavier [22] which is used in subsequent chapters.

Chapter 6 gives the design space and design of experiment study parameters which will be used while building surrogate model in Section 6.3. Running the actual CFD simulations for building surrogate model of CFD is done in Section 6.3. Chapter 7 explains the concept of hoop stress and also gives the methodology to calculate it as given by Alam [2]. The results obtained while performing multi-disciplinary optimization of aerodynamic drag combined with hoop stress are presented in Chapter 8.

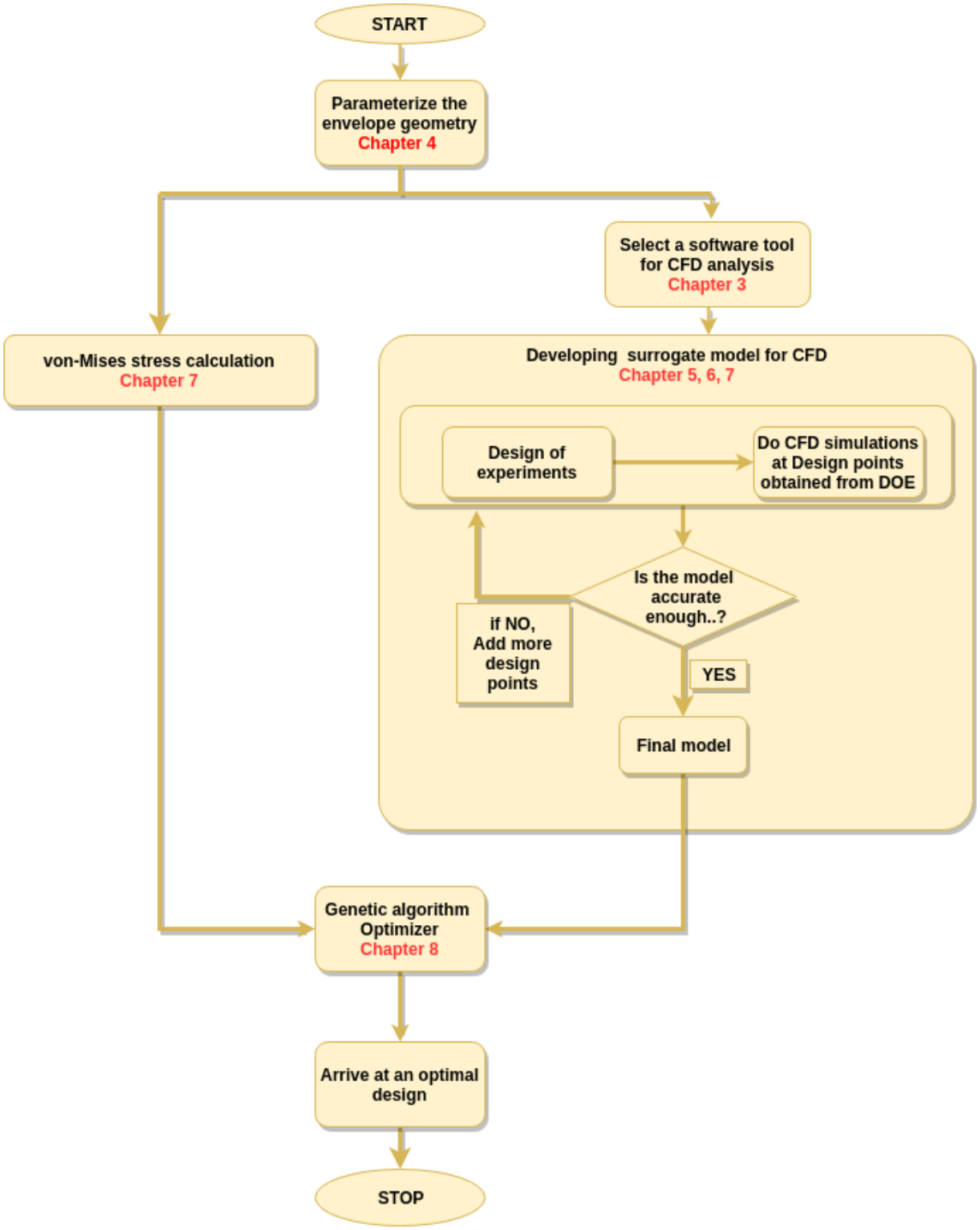

Figure 1.2: Framework of multi-disciplinary shape optimization

Next Chapter gives brief literature survey that has been carried out to understand the previous research carried out in the field of High Altitude Airships (HAA's) and shape optimization.

Chapter 2

Literature Survey

This chapter presents the research carried out by different individuals in the field of shape optimisation.

Ghani[11] used Non Uniform Rational B-Splines (NURBS) for envelope geometry parameterization of passenger car and constructed a response surface model on the geometries to obtain drag coefficients. Finally, the design exploration was performed using the response surface model instead of actual CFD simulations.

Alam[1] selected *Gertler Series-58* [10] shape generation for optimization studies, in which the envelope shape is driven by four shape parameters and fineness ratio. Wang et al.[34] proposed a geometry parameterization algorithm for axisymmetric bodies using four shape parameters namely *a,b,c,d* and length *l*.

Kanikdale et al.[16] has taken GNVR shape [21] as baseline reference and validated their ANSYS® *Fluent* results with it. Geometry has been parameterized using six design parameters and response surface based on CFD results was fitted. With low fidelity analysis using the formula by Gillett et al.[5]. An improvement of 1.3 % was observed in C_{DV}. Whereas using CFD analysis, they found that the drag for optimized shape is 27 % greater than GNVR hull shape. By this, they concluded that the formula given by Gillet and Khoury cannot be used for optimization purpose.

Kale et al.[15] proposed a generic methodology for determination of drag coefficient of an aerostat envelope using CFD. The envelope was parameterized in terms of six geometric coefficients, and a shape generation algorithm was developed. They have studied around 600 feasible shaped using ANSYS® *Fluent* CFD package and fitted a quadratic response surface using Design-Expert package. They taken a composite objective function involving aerodynamic drag, structural stress and surface area (so weight) of the envelope. They have observed that the location of maximum thickness affects the drag mostly.

Ram et al.[27] parameterized the shape using the formulation proposed by Kanikdale et al.[16] and arrived at optimum shape using hybrid Genetic Algorithm (GA). The objective function was to maximize its payload while incorporating considerations of aerodynamics, structures and flight mechanics.

Wang et al.[34] have tested a scaled down model of Zhiyuan - 1 airship in a 3.2 m diameter wind tunnel and installed roughness strips on the surface of hull to trip the flow from laminar to turbulent. They studied the effect of lengthwise location of these strip on the its aerodynamic characteristics at different angles of attack and side slip. They have reported large sets of experimental data for bare hull, hull with fins and hull with fins, gondola. They concluded that the drag almost doubled because of change of flow condition from laminar to turbulent.

Suman et al.[30] tried to reproduce the experimental results of Wang et al.[34] using computational fluid dynamics. To simulate the turbulence strips installed by Wang et al.[34] on the surface of the hull, Suman et al.[30] modeled transition location in CFD which changes the flow from laminar to turbulent. It has been observed that although Wang et al.[34] provided strips at the leading edge, the flow has not been tripped to turbulent because of favorable pressure gradient.

Comprehensive results for the effect on size and payload capability of airship of various factors like, altitude, latitude, pressure difference, helium purity etc. has been published by Chen et al.[7]. The calculation is carried out for NPL shape.

Liu et al.[17] carried out numerical calculations about the test model to investigate the aerodynamics behaviour. They confirmed the lower drag behaviour of *Zhiyuan-1* airship. They discussed the influence of gondola and fins on the pressure distribution.

Ceruti et al.[4] defined a shape which is non body of revolution using five design parameters. They have found the drag coefficient for 10 such combinations of design parameters and used interpolation based approach for estimation of drag coefficient of any given shape. They used different optimization techniques to arrive at a configuration of minimum drag and weight.

2.1 Recent work in the field

A brief summary of recent work done by Alam [2] in the field of multi-disciplinary shape optimization is given below.

Surrogate model for CFD analysis: For CFD analysis, 60 simulations have been carried out and fitted into the *Kriging* surrogate model toolbox developed by Viana et

al.[32]. This has been coupled with the optimizer without having the need to do CFD routine every time.

Shape generation algorithm: The shape generation algorithm proposed by Gertler[10] called *Gertler Series 58 Shape Generator* has been used instead of that by Wang et al.[34]. Efficacy of this shape generator has been demonstrated by capturing different standard airship shapes.

Sizing and Optimization: A new sizing methodology has been developed by Alam et al.[3] and optimization has been carried out using MATLAB Global optimization Toolbox and SIMANN optimizer.

The next chapter investigates envelope shape generation algorithms for non-axisymmetric shapes because the existing literature has only algorithms for axisymmetric shapes.

Chapter 3

Introduction to OpenFOAM®

OpenFOAM® is an open source software where we can get the source code along with binary executable for all the solvers. The FOAM project (precursor to OpenFOAM®) was created at Imperial College London in the late 80s and early 90s by Henry Weller, along with Hrvoje Jasak [13], using object-oriented programming language C++. Succeeding the commercial software FOAM, OpenFOAM® was released in 2004 as free and open-source software under the GNU General Public License (GPL), a widely used free software license, which guarantees end users the freedom to run, study, share and modify the software. Here we can modify the existing solvers, compile them and add to the library. One distinguishing feature of OpenFOAM® is its syntax for tensor operations and Partial Differential Equations (PDEs) that closely resembles the equation being solved. For example, the equation:

$$\frac{\partial(\rho U)}{\partial t} + \nabla \cdot \phi U - \nabla \cdot \mu \nabla U = -\nabla p \tag{3.1}$$

is represented by the code:

```
Solve
(
fvm :: ddt(rho,U)
+ fvm :: div(phi,U)
- fvm :: laplacian(mu,U)
==
-fvc :: grad(p)
);
```

Thus we can see that all the mathematical operators like divergence, curl, gradient, laplacian etc. are well defined in OpenFOAM®. OpenFOAM® treats fluid, structural,

thermal or acoustic or any other field problems in the exactly same way as long as there are governing equations in them and they can be written in conservative form. It uses finite volume discretization method. Whenever we are programming any new solver, 90 percent of the code remains same with baseline solver and changes to be made are less than 10 percent. Thus using OpenFOAM®, there is no need to write the entire code right from scratch every time. We can just edit the existing solver and save lot of time.

Automatic mesh generation utility called *SnappyHexMesh* comes along with OpenFOAM® where in we have to give .stl or .obj file of geometry and specify the domain, mesh size and level of refinement needed. Rest of the tasks are automated. This is particularly useful when we have to couple CFD analysis to the optimizer. *SnappyHexMesh* is still in development phase and is getting better with every release.

The absence of Graphical User Interface (GUI) can be taken as an advantage because we come to know the actual physics of flow happening behind the scene. If we become moderately expert in OpenFOAM® then it saves a lot of time because every process can be programatically controlled from mesh generation to post processing.

OpenFOAM® comes with a Open Source CFD post processing utility known as *ParaView* which is a scientific data visualization software. Since we solve Navier Stokes equations using Finite Volume Approach, at the end of simulation, we are provided with data at the center of cells. *ParaView* has many post-processing options called filters which can be applied and desired plots can be drawn.

3.1 Computational mesh generation using *SnappyHexMesh*

SnappyHexMesh is a hexahedral unstructured mesh generation tool included in the distribution of OpenFOAM®. *SnappyHexMesh* can use a 3-D .stl surface and iteratively build a mesh upon it. Some options allow construction of several cell layers of a controllable height above the 3D surface.This feature makes it possible to have a refined mesh in the region of high velocity gradients, close to the surface. Near the surface, the mesh is refined and cells are splitted acoordingly. The process is explained in Fig. 3.1 .Several regions can be selected to be refined to a desired level, and this method creates mesh of a cell aspect ratio close to 1.This is done in order to ensure that OpenFOAM® can solve the numerical problems with the highest efficiency and accuracy using meshes generated with *SnappyHexMesh*. The meshing tool *SnappyHexMesh* can be run in parallel on a computer cluster or a PC.

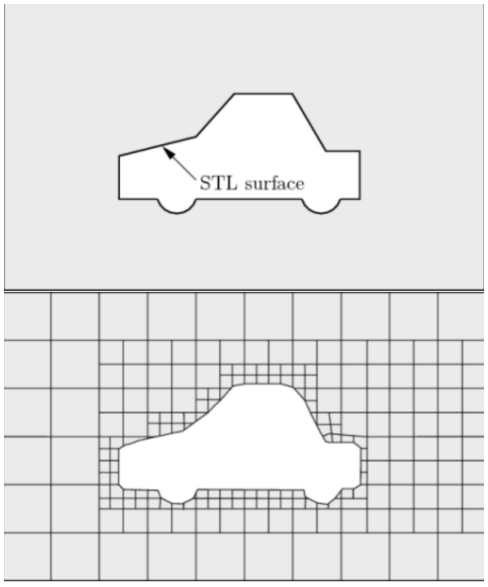

Figure 3.1: Surface snapping process in *SnappyHexMesh* [25]

Although in the Fig. 3.1, it is shown for 2D, *SnappyHexMesh* is a 3D meshing utility. It also provide options to add viscous layers to resolve boundary layer. We can also control the thickness of first layer. This thickness of first layer is usually determined by Yplus value which is a dimensionless wall thickness. A non-dimensional wall distance for a wall-bounded flow can be defined in the following way:

$$y^+ \equiv \frac{u_* y}{\nu} \tag{3.2}$$

Where u_* is the friction velocity at the nearest wall, y is the distance to the nearest wall and ν is the local kinematic viscosity of the fluid.

y^+ is often referred to simply as y plus and is commonly used in boundary layer theory and in defining the law of the wall.

Fig. 3.2 shows the mesh near the surface of an arbitrary airship shape to resolve the boundary layer.

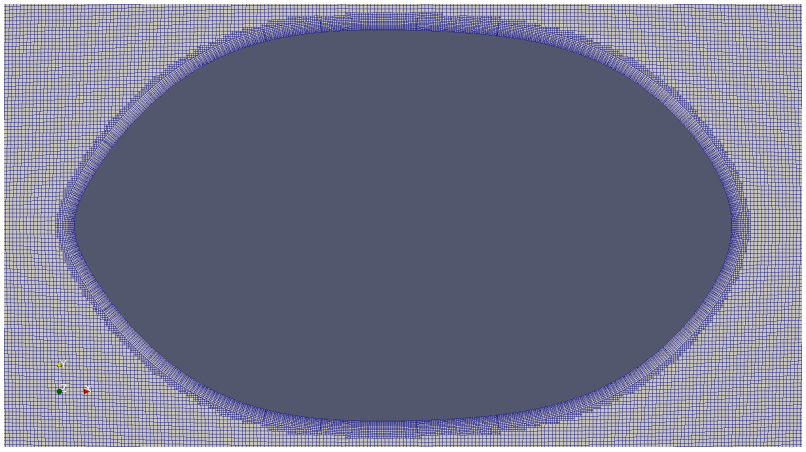

Figure 3.2: Prism layers on the surface of GNVR to capture boundary layer

3.2 Validation of OpenFOAM® CFD results

This section describes the values of C_{DV} obtained for four standard axisymmetric Lighter Than Air (LTA) envelope shapes, viz., GNVR [27], NPL 5 Zhiyuan-1 34, and Wang 33, using OpenFOAM®, and a comparison with the values available from the literature. Fig. 3.3 shows these four profiles. All the simulations were carried at zero degree angle of attack.

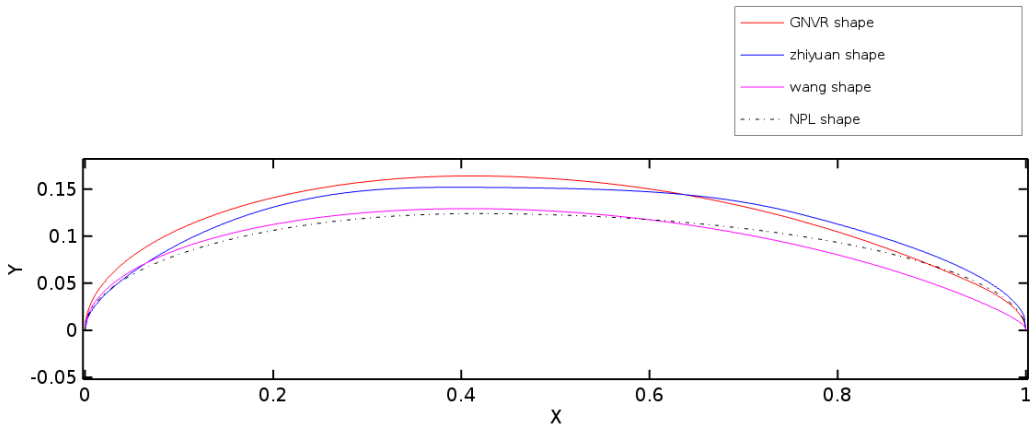

Figure 3.3: Four standard shapes available in literature

The specifications of machine, operating system, and software used in this study are as follows:

- Model name = Intel(R) Xeon(R) CPU E5-2650
- Number of physical cores = 40

- Processor speed = 2.8 GHz
- Operating system = Cent OS 7.4
- OpenFOAM® version = 4.1

Following subsections shows flow conditions, solver parameters and results of CFD simulation carried on the above mentioned standard shapes.

3.2.1 GNVR shape

The GNVR shape 27 is named after late Prof. G.N.V Rao of Indian Institute of Science, Bengaluru. It consists of three standard geometrical constructs, viz, ellipse, circle and parabola. The entire envelope shape is parameterized in terms of its maximum diameter (D), as follows:

$$y = \begin{cases} 0.5D\sqrt{1-(\frac{X-1.25D}{1.25D})^2} & 0 < X < 1.25D \\ \sqrt{16D^2-(X-1.25D)^2}-3.5D & 1.25D \leq X \leq 2.875D \\ \sqrt{0.1373D(1.8D-(X-1.25D))} & 2.875D \leq X \leq 3.05D \end{cases} \tag{3.3}$$

The flow conditions used for the simulation are similar to that of Kanikdale *et al.* [16]. Taking advantage of the axisymmetric nature of GNVR shape, its 3D CFD analysis was carried out only for 1/4 of its shape. The flow conditions and solver parameters are shown in Table 3.1

Table 3.1: Flow conditions and solver parameters for GNVR shape

Flow Conditions	Solver parameters
$Velocity = 50.339\ m/s$	$Number\ of\ cells = 646,639$
$Pressure = 101325\ Pa$	$Number\ of\ parallel\ cores = 20$
$Density = 1.225\ kg/m^3$	$Time\ taken\ for\ solution = 475\ s$
$Reynolds\ number = 34.783 * 10^6$	
$Turbulence\ model = k-\epsilon$	

The variation of Pressure coefficient (C_P) along the envelope length obtained using OpenFOAM® is compared with that of using ANSYS® *Fluent* by Kanikdale et al. [16] and Panel Method by Narayana and Srilatha [21].

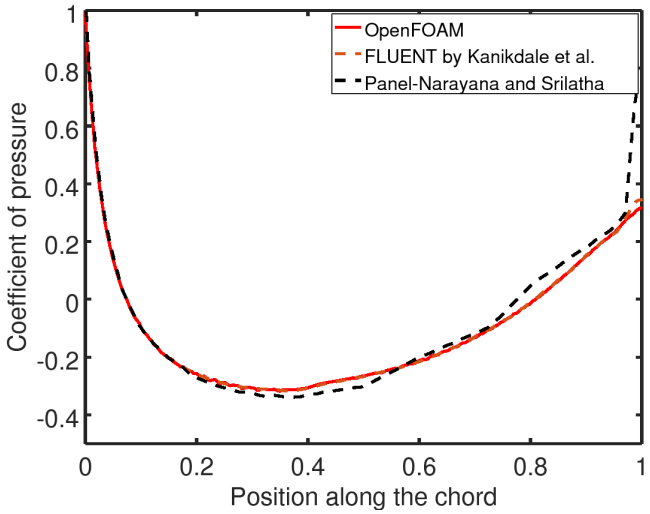

Figure 3.4: C_P distribution for GNVR profile obtained by OpenFOAM®, Source Panel Method [21] and ANSYS® *Fluent* [16]

It can be observed from Fig. 3.4 that the C_P distribution obtained by OpenFOAM® matches well with that obtained by ANSYS® by Kanikdale et al. [16] along the entire envelope length, except at the trailing edge, where the flow is separated. The distribution obtained by Source Panel Method [21] shows very high pressure recovery at trailing edge because it is assumed that *Kutta* condition is satisfied and flow is attached.

3.2.2 Zhiyuan-1 shape

The equation that define the Zhiyuan-1 shape is:

$$y = \begin{cases} f_r'[r_n F_1(z) + k_1 F_2(z) + G(z)]^{\frac{1}{2}} & \begin{array}{l} For: 0 < x \leq x_m \\ F_1(z) = -2z(z-1)^3 \\ F_2(z) = -z^2(z-1)^2 \\ G(z) = z^2(3z^2 - 8z + 6) \end{array} \quad z = \frac{x}{x_m} \\ \hline f_r'[s_t^2 F_1(z) + \left(\frac{1-x_m}{x_m}\right)^2 k_1 F_2(z) + G(z)]^{\frac{1}{2}} & \begin{array}{l} For: x_m < x \leq x_p \\ F_1(z) = -z^2(z-1)^3 \\ F_2(z) = -z^3(z-1)^2 \\ G(z) = z^3(6z^2 - 15z + 10) \end{array} \quad z = \frac{1-x}{1-x_m} \\ \hline f_r'[c_p(1-z)]^{\frac{1}{2}} & For: x_p < x \leq 1 \quad z = x \end{cases}$$

Values of the constants mentioned above are $x_m = 0.393591$, $x_p = 0.7570323$, $r_n = 0.5070992$, $k_1 = 0.291256$, $c_p = 2.735107$, $f_r^{'} = 0.1515518$ *and* $s_t = 3.236105$. Suman

et al. [30] carried out a Reynolds-Averaged Navier - Stokes (RANS) simulation to reproduce the results obtained by Wang *et al.* [34] for transition assumed at the leading edge itself, i.e., for a fully turbulent flow. They have also obtained results for various assumed locations of the transition points, resulting in pockets of laminar and turbulent regions in the computational domain.

In the present study, a 3-D CFD analysis for Zhiyuan-1 shape was carried out and pressure distribution obtained is shown in Fig. 3.5.

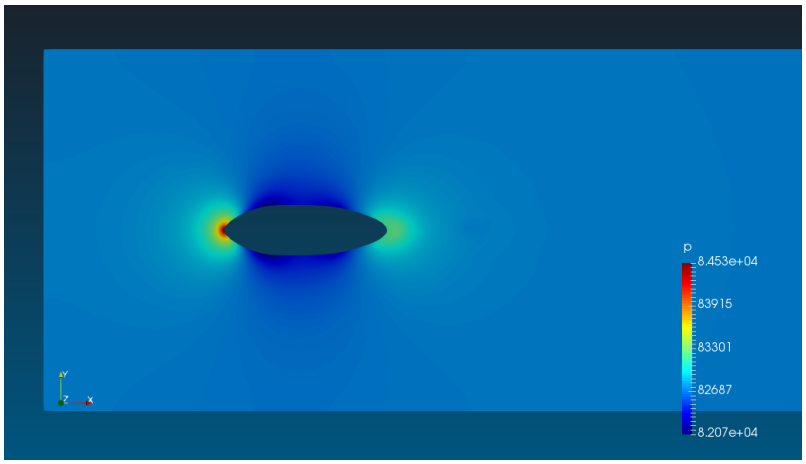

Figure 3.5: Pressure distribution on Zhiyuan-1 airship shape

The results were obtained only for one half of the envelope and 'SymmetryPlane' boundary condition was incorporated for the other half to reduce the computational time.

The flow conditions used for the simulation were same as used by Suman et al.[30] and Wang et al. [34] and is given in Table 3.2

Table 3.2: Flow conditions and solver parameters for Zhiyuan-1 shape

Flow Conditions	Solver parameters
$Velocity = 60.39\ m/s$	$Number\ of\ cells = 2,982,639$
$Pressure = 101325\ Pa$	$Number\ of\ parallel\ cores = 8$
$Density = 1.225\ kg/m^3$	$Time\ taken\ for\ solution = 4534\ s$
$Reynolds\ number = 2.4 * 10^6$	
$Turbulence\ model = \kappa\omega\ SST$	

Fig. 3.6 shows a comparison between the C_P distribution for Zhiyuan-1 envelope shape using OpenFOAM® with ANSYS® *Fluent* and experimental results quoted by Wang *et al.* [34].Table 3.3 compares the components of C_{DV} obtained using OpenFOAM® and RANS [30].

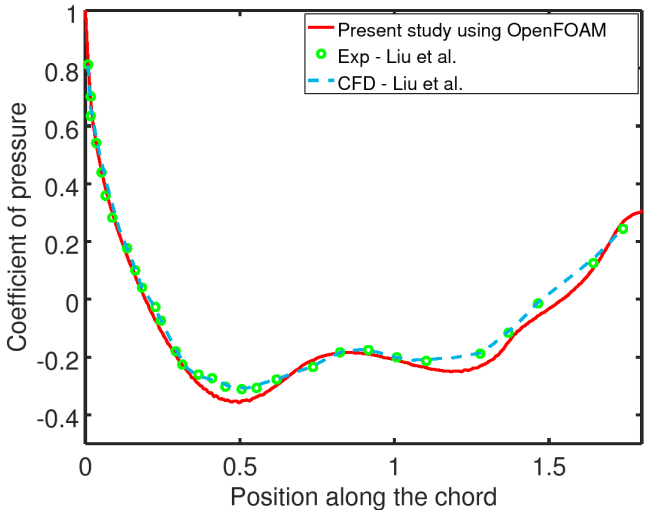

Figure 3.6: C_P distribution for Zhiyuan-1 shape using OpenFOAM®, Experiments [34] and ANSYS® *Fluent* [34]

Table 3.3: Comparison of OpenFOAM® results with RANS [30] for Zhiyuan -1 shape

	OpenFOAM®	RANS [30]	% error
$C_{DV}(Viscous)$	0.01989	0.01890	5.3
$C_{DV}(Pressure)$	0.00583	0.00568	2.8
$C_{DV}(Total)$	0.02573	0.02456	4.8

3.2.3 Wang Shape

Wang et al. [33] proposed a new shape exploring the better shapes in the view of multi-disciplinary optimization. The geometry is defined by five shape parameters namely *a, b, c, d* and length *l*. The original equation proposed by Wang *et al.*[33] is given by Eq. 3.4:

$$64(y^2 + z^2) = a(l - x)\left(bx - l\sqrt{c} + \sqrt{cl^2 - dlx}\right) \tag{3.4}$$

The values taken for the parameters of Wang shape are $a = 7.447$, $b = 2.072$, $c = 9.010$, $d = 7.981$ *and* $l = 194.0$. For the sake of convenience, geometry is scaled down by length (l) in all directions. Wang shape defined by Eq. 3.4 is a body of revolution and also can be obtained by rotating the profile given by Eq. 3.5 through 360^o. The flow conditions and solver parameters used for the simulation are shown in Table 3.4:

$$y = \frac{\sqrt{a(l - x)\left(bx - l\sqrt{c} + \sqrt{cl^2 - dlx}\right)}}{8} \tag{3.5}$$

Table 3.4: Flow conditions and solver parameters for Wang shape

Flow Conditions	Solver parameters
$Velocity = 51\ m/s$	$Number\ of\ cells = 1,060,202$
$Pressure = 8750\ Pa$	$Number\ of\ parallel\ cores = 8$
$Density = 1.225\ kg/m^3$	$Time\ taken\ for\ solution = 2865\ s$
$Reynolds\ number = 3.01 * 10^6$	
$Turbulence\ model = SpalartAllmaras$	

The values obtained for finer grid case using OpenFOAM® are compared with those of using ANSYS® *Fluent*. Fig. 3.7 shows the comparison of C_P distribution.Table 3.5 shows the comparison of C_{DV} obtained using OpenFOAM® and ANSYS® *Fluent*

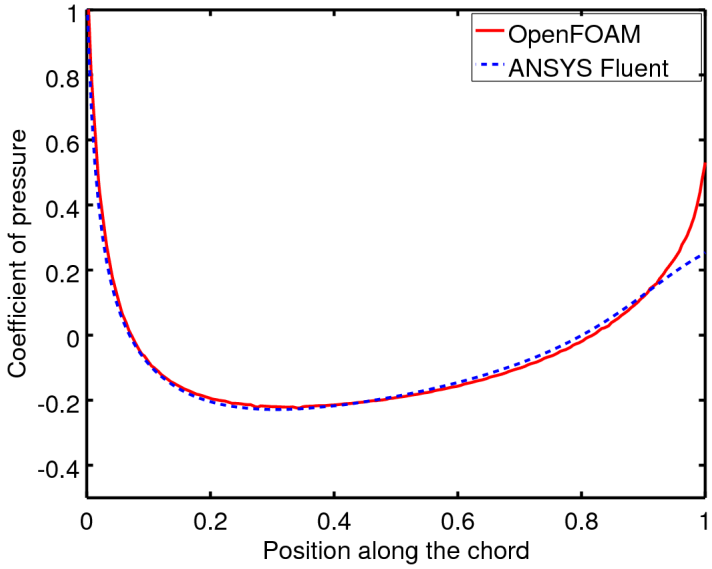

Figure 3.7: Comparison of OpenFOAM® results with ANSYS® *Fluent* results for pressure distribution of Wang shape

Table 3.5: Comparison of OpenFOAM® results with ANSYS® *Fluent* for Wang shape

	OpenFOAM®	ANSYS® *Fluent*	% error
C_{DV}	0.02730	0.02610	4.6

3.2.4 NPL Shape

NPL shaped envelope is basically the combination of two half prolate joint at maximum diameter. It is known for its lower drag characteristics. The mathematical represen-

tation of prolate is:

$$\frac{x^2}{a^2} + \frac{y^2}{b^2} + \frac{z^2}{c^2} = 1 \tag{3.6}$$

The same surface given by Eq.3.6 can also be obtained by rotating the curve given by Eq.3.7 along X axis

$$y = \begin{cases} \pm b\sqrt{1 - \dfrac{(x-a)^2}{a^2}} & When\ x \leq a \\ \pm b\sqrt{1 - \dfrac{(x-a)^2}{2a^2}} & When\ x \leq a \end{cases} \tag{3.7}$$

Values of constants mentioned above are: $a = 82.485 \quad and \quad b = 24.681$

For the sake of convenience, The surface generated is scaled down by length (l) in all directions.The values obtained for finer grid case using OpenFOAM® are compared with those of using ANSYS® *Fluent*.

The flow conditions and solver parameters used for the simulation are shown in Table 3.6

Table 3.6: Flow conditions and solver parameters for NPL shape

Flow Conditions	Solver parameters
$Velocity = 51\ m/s$	$Number\ of\ cells = 1,063,736$
$Pressure = 87500\ Pa$	$Number\ of\ parallel\ cores = 8$
$Density = 1.057\ kg/m^3$	$Time\ taken\ for\ solution = 2701\ s$
$Reynolds\ number = 3.01 * 10^6$	
$Turbulence\ model = Spalart\ Allmaras$	

Fig. 3.8 shows the comparison of C_P distribution using OpenFOAM® and ANSYS® *Fluent*. Table 3.7 shows the comparison of C_{DV} obtained using OpenFOAM® and ANSYS® *Fluent*.

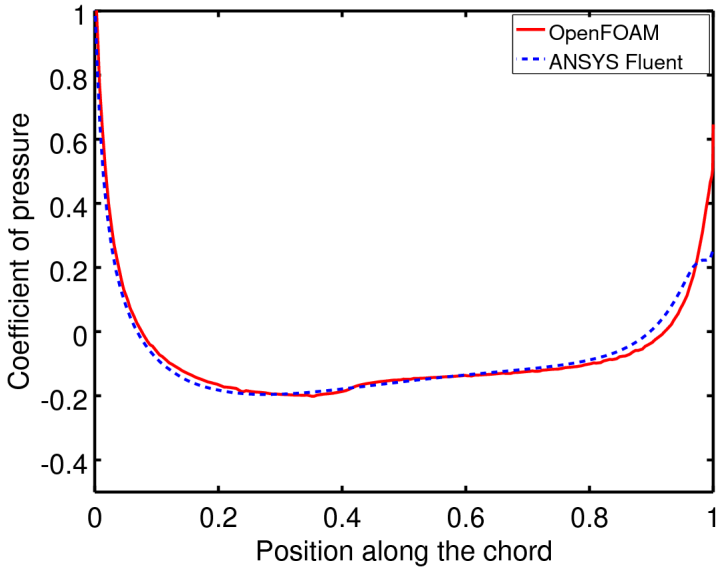

Figure 3.8: Comparison of OpenFOAM® results with ANSYS® *Fluent* results for pressure distribution of NPL profile [6]

Table 3.7: Comparison of OpenFOAM® results with ANSYS® *Fluent* for NPL shape

	OpenFOAM®	ANSYS® *Fluent*	% error
C_{DV}	0.02598	0.02660	2.3

3.2.5 Grid Dependence study

Since the solution is influenced by mesh size, three self similar grids with increasing number of grid points were considered. Table 3.8, 3.9 and 3.10 compares the value for C_{DV} obtained using OpenFOAM® for GNVR [27], Wang [33] and NPL[6] shapes respectively.

Table 3.8: Grid Dependence study for GNVR shape

	No. of cells	C_{DV} using OpenFOAM®	% error change
Coarse	198315	0.01565	NA
Fine	646543	0.01555	0.6
Veryfine	1444016	0.01572	1.1

Table 3.9: Grid Dependence study for Wang shape

	No. of cells	C_{DV} using OpenFOAM®	% error change
Coarse	1516763	0.02709	NA
Fine	2494963	0.02597	10.2
Veryfine	2808841	0.02496	7.9

Table 3.10: Grid Dependence study for NPL shape

	No. of cells	C_{DV} using OpenFOAM®	% error change
Coarse	220813	0.02709	NA
Fine	1520195	0.02597	4.1
Veryfine	2521622	0.02496	3.8

According to Suman et al. [30] if percentage changes compared to previous grid is $\leq$ 5% then the value obtained from latest grid can be considered as the most accurate. From the above tables we may observe that for GNVR and NPL profiles, the percentage changes are < 5 %, however for Wang profile, they are >5 %. Thus, we can observe that the solution is nearly independent of grid size in all the cases.

3.3 Observations & Conclusions

From the above results we can observe that OpenFOAM® results match quite well with those obtained using commercial software like ANSYS® *Fluent* and other proprietary software like RANS [30]. The likely reasons for the minor differences in the values are as follows:

- The results available in literature are 2D simulations using ANSYS® *Fluent* whereas in our case, they are 3D simulations using OpenFOAM®.
- The values of some parameters (e.g., wall functions and wall boundary conditions) had to be assumed because they were not listed in the literature.

Apart from the above reasons, OpenFOAM® solver implementation are different from those of ANSYS® *Fluent*. Only a more detailed and systematic computational study and comparison with reliable experimental data can totally establish the efficacy of OpenFOAM® w.r.t. ANSYS® *Fluent* and other proprietary codes. In last three Chapters, essential tools to carry out shape optimization like geometry, mesh and solver has been discussed. The methodology for optimization is discussed in next Chapter.

Chapter 4

Envelope geometry parameterization

Geometry parameterization is an essential part of the design exploration and shape optimization process and there are several methods of generating parametric geometries. Since our ultimate aim of the project is to study different configurations of the non-body-of-revolution shapes and select the best one satisfying our needs. Thus there is a need to parameterize the geometry. Initial attempts were made using unconventional generalised methods like polynomial fitting, ruled surface between splines, NURBS etc. The idea is to define any shape using design variables of not more than 10 because the complexity (time taken, number of function evaluations and memory consumption) of an optimizing problem increases exponentially[11] with number of design variables. So, it has to be as less as possible provided every combination of them gives a meaningful airship shape.

4.1 Modified Gertler parameter technique

In this study, Gertler Series 58 Shape Generator are used for airship envelope generation. This sub-section explains the formulation of this shape generator in detail. It starts with a six degree polynomial equation in 2-D as stated in Eq. 4.1.

$$z^2 = a_1 y + a_2 y^2 + a_3 y^3 + ... + a_n y^n \tag{4.1}$$

where a_1, a_2, a_3,..., a_n are the shape coefficients, whose values are driven by geometrical parameters, viz., m (location of maximum diameter), r_o (Nose radius), r_1 (tail radius) and C_p (prismatic coefficient), shown in Fig. 4.1. Here V_{env} is the volume of the envelope and V_c is volume of enclosing cylinder.

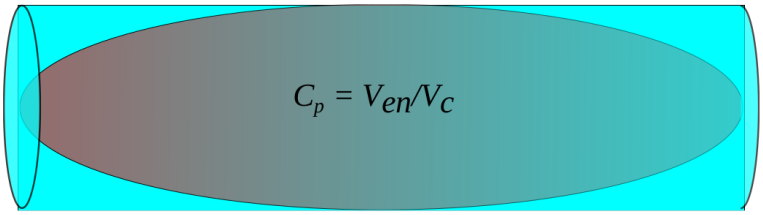

Figure 4.1: Definition of Cp [2]

By satisfying the various constraints applicable for the shape of a stratospheric airship envelope, the final equations can be obtained in terms of these shape coefficients. To satisfy the constraints applicable for an airship envelope, we apply the conditions $z = 0$, when $y = 1$; $z = 1/2$, when $y = m$ and $\frac{dz}{dy} = 0$, when $y = m$, to obtain:

$$a_1 + a_2 + a_3 + ... + a_n = 0 \tag{4.2}$$

$$a_1 m + a_2 m^2 + a_3 m^3 + ... + a_n m^n = \frac{1}{4} \tag{4.3}$$

$$a_1 + 2a_2 m + 3a_3 m^2 + ... + n a_n m^{n-1} = 0 \tag{4.4}$$

Radius of curvature R for any curve can be given as:

$$R = \pm \frac{1}{\frac{d^2Y}{dZ^2}} \left[1 + \left(\frac{dY}{dZ}\right)^2\right]^{3/2} \tag{4.5}$$

Eq. 4.5 can be expressed in a dimensionless form as:

$$r = \pm \frac{1}{\frac{d^2y}{dz^2}} \left[1 + \frac{L^2}{D^2}\left(\frac{dy}{dz}\right)^2\right]^{3/2} \tag{4.6}$$

Differentiating Eq. 4.1 successively with respect to y we get:

$$2z = \left(a_1 + 2a_2 y + ... + n a_n^{n-1}\right) \frac{dy}{dz} \tag{4.7}$$

and

$$2 = \left(a_1 + 2a_2 y + ... + n a_n^{n-1}\right) \frac{d^2y}{dz^2} + \left[2a_2 + ... + n(n-1) a_n^{n-2}\right] \left(\frac{dy}{dz}\right)^2 \tag{4.8}$$

In Eq. 4.7, if $a_1 \neq 0$ then it can be said that when $x = 0$, $\frac{dy}{dz} = 0$, and hence from the Eq. 4.8, that $\frac{d^2y}{dz^2} = \frac{2}{a_1}$. Consequently substituting these values in Eq. 4.6 we can get:

$$a_1 = 2r_o \tag{4.9}$$

where r_o is the radius of curvature at the nose. If, on the other hand $a_1 = 0$, then $r_o = 0$, i.e., the body has pointed nose, which is not possible for an inflated envelope. Hence, Eq.

4.9 is valid for both the cases.
Similarly, when $y = 1, z = 0$ and from Eq. 4.7, $\frac{dy}{dz} = 0$, unless:

$$a_1 + 2a_2 + 3a_3 + ... + na_n = 0 \tag{4.10}$$

Hence, Eq. 4.6 and Eq. 4.8 give:

$$a_1 + 2a_2 + 3a_3 + ... + na_n = -2r_1 \tag{4.11}$$

where r_1 is the radius of curvature at the tail. Different signs are taken in equation of r_o and r_1 because of the nature of slope at the points $y = 0$ and $y = 1$ respectively.

Volume of the envelope (V_{env}) can be expressed as:

$$V_{env} = \int_0^l \pi Z^2 dY = \pi d^2 L \int_0^1 z^2 dy \tag{4.12}$$

substituting for z^2 from Eq. 4.1 we get,

$$\frac{1}{2}a_1 + \frac{1}{3}a_2 + \frac{1}{4}a_3 + ... + \frac{1}{n+1}a_n = \frac{1}{4}C_p \tag{4.13}$$

The aforementioned six constraints can be expressed in the form of a six degree polynomial as follows:

$$z^2(0) = 0 \tag{4.14}$$

$$z^2(1) \implies a_1 + 2a_2 + 3a_3 + ... + na_n = 0 \tag{4.15}$$

$$\left.\frac{dz}{dy}\right|_0 \implies a_1 = 2r_o \tag{4.16}$$

$$\left.\frac{dz}{dy}\right|_1 \implies a_1 + 2a_2 + 2a_3 + ... + na_n = -2r_1 \tag{4.17}$$

$$z^2(m) \implies a_1 m + a_2 m^2 + a_3 m^3 + ... + a_n m^n = \frac{1}{4} \tag{4.18}$$

$$\left.\frac{dz}{dy}\right|_m \implies a_1 + 2a_2 m + 3a_3 m^2 + ... + na_n m^{n-1} = 0 \tag{4.19}$$

$$\int_0^1 z^2(y)dy \implies \frac{1}{2}a_1 + \frac{1}{3}a_2 + \frac{1}{4}a_3 + ... + \frac{1}{n+1}a_n = \frac{1}{4}C_p \tag{4.20}$$

The above-mentioned linear equations can be represented in a Matrix form as:

$$A\boldsymbol{Y} = B \tag{4.21}$$

$$\begin{bmatrix} 1 & 1 & 1 & 1 & 1 & 1 \\ 1 & 0 & 0 & 0 & 0 & 0 \\ 1 & 2 & 3 & 4 & 5 & 6 \\ m & m^2 & m^3 & m^4 & m^5 & m^6 \\ 1 & 2m & 3m^2 & 4m^3 & 5m^4 & 6m^5 \\ \frac{1}{2} & \frac{1}{3} & \frac{1}{4} & \frac{1}{5} & \frac{1}{6} & \frac{1}{7} \end{bmatrix} \begin{bmatrix} a_1 \\ a_2 \\ a_3 \\ a_4 \\ a_5 \\ a_6 \end{bmatrix} = \begin{bmatrix} 0 \\ 2r_o \\ -2r_1 \\ \frac{1}{4} \\ 0 \\ \frac{1}{4}C_p \end{bmatrix}$$

There are six unknowns in these six linear equations, hence $\boldsymbol{Y}$ can be obtained for a set of geometrical parameters by solving these equations simultaneously. The final equation for airship envelope shape can be rewritten as:

$$z(y) = D\sqrt{a_1\left(\frac{y}{L}\right) + a_2\left(\frac{y}{L}\right)^2 + a_3\left(\frac{y}{L}\right)^3 + a_4\left(\frac{y}{L}\right)^4 + a_5\left(\frac{y}{L}\right)^5 + a_6\left(\frac{y}{L}\right)^6} \tag{4.22}$$

The obtained curve is then rotated about X-axis to get axisymmetric shape. However to get a non axisymmetric shape, we introduce a new variable called $scale_y$ which when multiplied with the y-coordinates of the body changes it into non-axisymmetric shape. The below figure shows the effect of scaling.

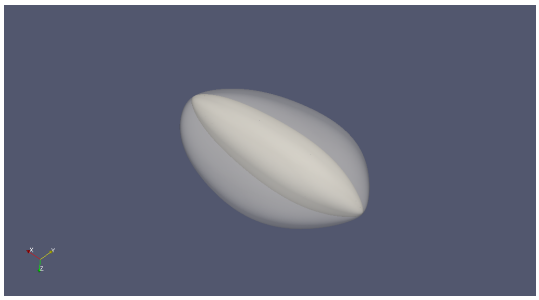

Figure 4.2: Effect of scaling

4.2 Methodology to generate geometry using *Octave*

Since the analysis work is being carried out using OpenFOAM®, we need to input the geometry file to *SnappyHexMesh* utility. OpenFOAM® does not have any geometry creation utility. It has to be created using any commercial designing software and file has to be exported in **.stl** format. During optimization, calling the commercial CAD software every time to define simple mathematical shape is not a good practice. Instead we can define the geometry in Octave itself and carryout simulations. So, an existing MATLAB® script by Bill [23] has been edited which takes the input of surface data (X,Y and Z vectors) and writes them into .stl file. This .stl file can then be used in OpenFOAM®. So, the need for commercial designing software has been eliminated.

4.2.1 STL (file format)

An ASCII STL file begins with the line

```
solid name
```

where name is an optional string (though if name is omitted there must still be a space after solid). The file continues with any number of triangles, each represented as follows:

```
facet normal ni nj nk
        outer loop
                vertex v1x v1y v1z
                vertex v2x v2y v2z
                vertex v3x v3y v3z
        endloop
endfacet
```

where each n or v is a floating-point number in sign-mantissa-"e"-sign-exponent format, e.g., "2.648000e-002". The file concludes with the line,

```
endsolid name
```

Thus the *surf* data consisting of x,y,z coordinates of all the points are written into a text file in the above format and can be imported into OpenFOAM® to carryout CFD simulation.

Chapter 5

Surrogate based shape optimization

The process employed for aerodynamic shape design can be a direct or indirect shape optimization. In direct shape optimization approach, the process starts with random combinations of design parameters. An optimization algorithm is used which requires CFD simulation at each iteration to find parameters in the design space for minimum drag. This approach requires large number of CFD simulations and takes significant amount of time to complete the optimization process. Also, grid influences the solution considerably. So, using this method we can no longer guarantee that the changes in the solution of objective function value is because of the changes in the parameters of CAD or if they are coming from changes in the grid. Solution for above problem can be answered by developing a surrogate model.

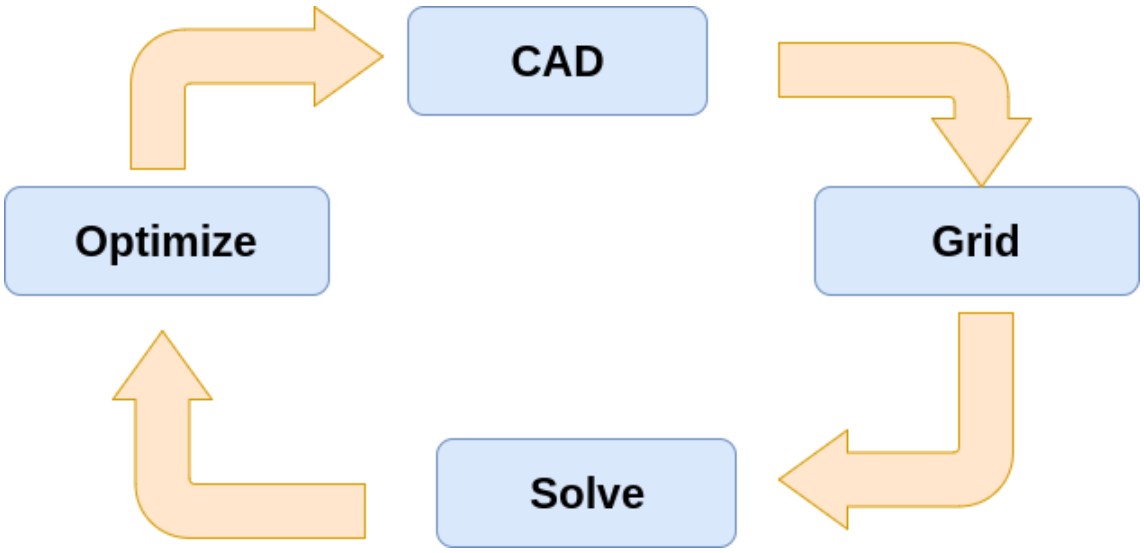

Figure 5.1: Direct shape optimisation approach

5.1 Surrogate model

Surrogate model is one of the mathematical and statistical techniques used to develop adequate functional relationship between an objective function y(x) and the control or design variables $x_1, x_2....x_k$. In our case, The model acts like a black box for aerodynamic parameters. Given the set of design variables, the model should give volumetric drag coefficient as shown in Fig. 5.1 . The work flow associated with the development of a surrogate model is shown in Fig. 5.3 . To develop an accurate surrogate, we need to carry out large number of CFD simulations. Creating geometry every time and meshing them is possible but takes a lot of time. Instead we can automate all the processes right from geometry creation to meshing and solving. This has become possible with OpenFOAM®.

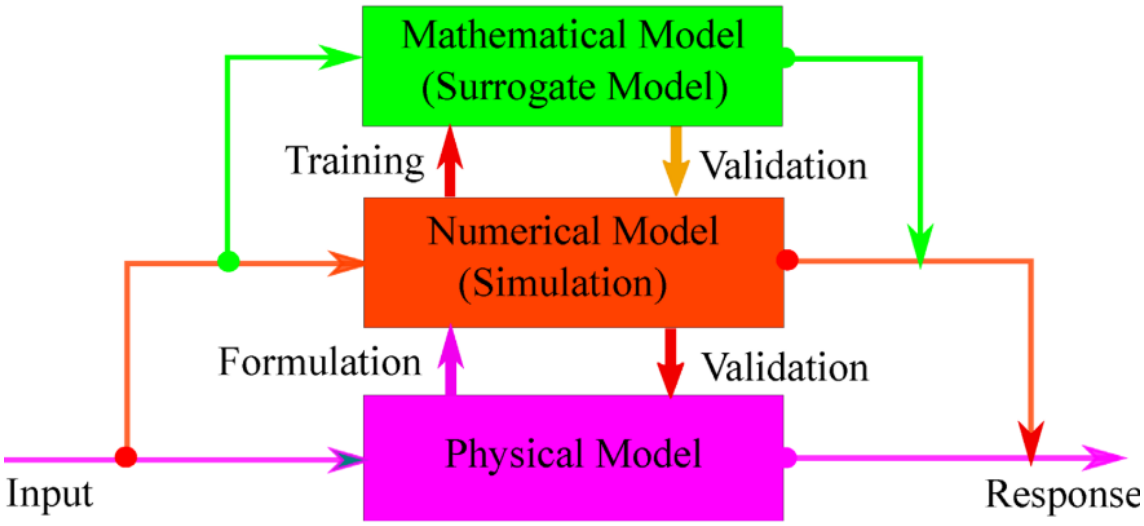

Figure 5.2: Surrogate model definition [2]

5.2 Design of Experiments

Design of Experiments is a technique used to extract maximum possible information from minimum number of computational experiments. This can be accomplished by the selection of a proper and robust scheme for DOE (Design of Experiments). In the present study, an open-source software named Surrogates Toolbox Version 3.0 (Viana, 2011) was used. Apart from many other important features, the toolbox provides an access to several varieties of widely used DOE models. Of the many DOE models available in the toolbox, Optimal Latin Hypercube Sampling (OLHS) generated using translational propagation

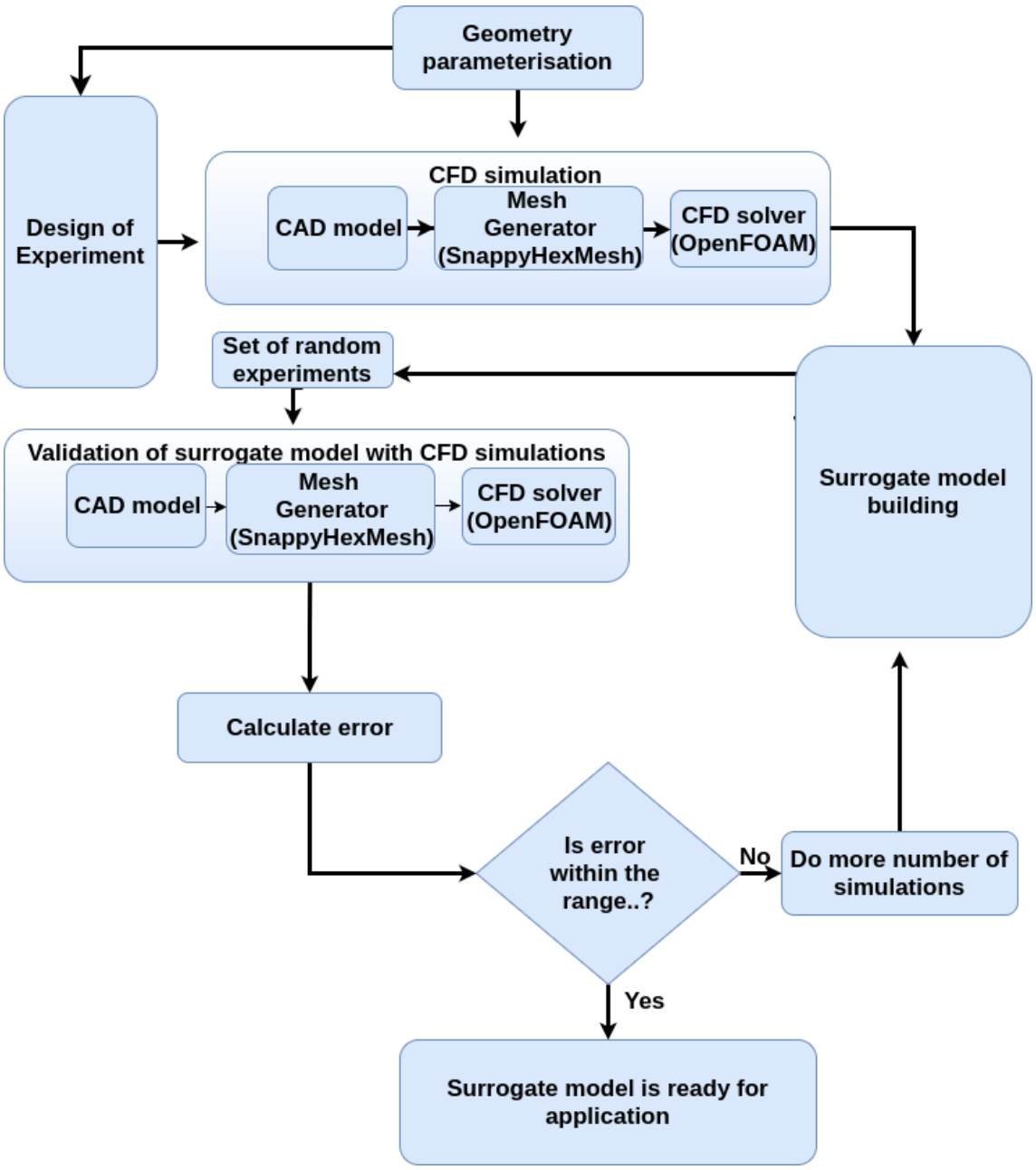

Figure 5.3: Work flow for the development of a surrogate model [11]

algorithm (TPA) Viana[31] was chosen, mainly due to its orthogonal structure. Fig. 5.4 shows sampling distribution of points in a unit square.

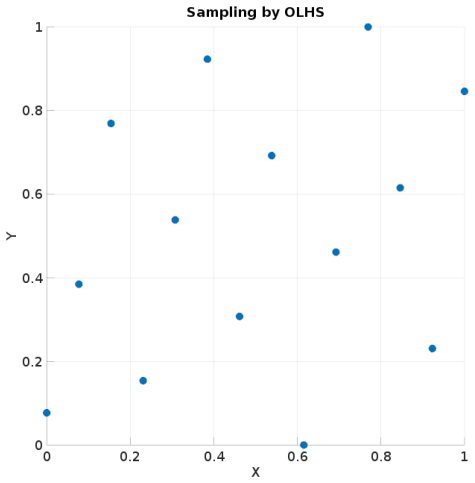

Figure 5.4: Sampling of unit square using OLHS

The number of design experiments depends on the number of shape parameters used for defining geometry. A rule of thumb is that the number of design experiments should be ten times the number of shape parameters. However the actual number is decided by obtaining error between surrogate model results and actual CFD results. For the surrogate model to be acceptable, the error should be less than 2 percent. Alam 1 reported to have made 60 design experiments while developing his surrogate model for 2D bodies of revolution shapes. Kale et al. [15] reported to have studied about 600 feasible shapes using ANSYS® *Fluent* CFD package while developing quadratic response surface using Design Expert package.

For numerical experiments, Kriging surrogate model is reported to be best 32. Kriging is named after the pioneering work of the South African mining engineer D. G. Krige. It is an interpolating method modeled by a Gaussian process governed by prior co-variances, which features the observed data at all design points. Kriging provides a statistic prediction of an unknown function by minimizing its Mean Squared Error (MSE).

The Kriging method in its basic formulation estimates the value of a function at some un sampled location as the sum of two components: the linear regression model $f_i(x)$ (e.g., polynomial trend) of the data with p regressors modeling the drift of the process mean, i.e., the trend, over the domain, and a systematic departure representing low (large scale) and high frequency (small scale) variation components, respectively.

5.3 Building the surrogate model

A brief overview of different surrogate models by Luo et al.[19] is given below.

5.3.1 Polynomial response surface

Polynomial response surface is the simplest approximation method to build surrogate models Forrester et al.[9]. The most widely used polynomial response surface model is the second-order polynomial model which has the following form.

$$y = \beta_0 + \sum_{i=1}^{n} \beta_i x_i + \sum_{i=1}^{n} \sum_{j \geq i}^{n} \beta_{ij} x_i x_j + .. \tag{5.1}$$

where β_0, β_i, β_{ii}, and β_{ij} are the regression coefficients, n is the number of variables, xi and xj are the variables. Using least square method (LSM), the regression coefficients can be solved.

5.3.2 Radial Basis Function

RBF is a 3-layer feed forward neural network consisting of an input layer, a hidden layer, and an output layer Shen et al.[29]. X is an N dimensional input vector. The output of the neurons in the RBF hidden layer is assumed as:

$$q_i = \Phi(\|X - c_i\|) \tag{5.2}$$

where c_i is the center associated with the ith neuron in the radial basis function hidden layer, i = 1, 2,...,H, where H is the number of hidden units, $\|X - c_i\|$ is the norm of Xc_i, $\Phi(.)$ is a radial basis function [8]. Outputs of the kth neuron in RBF output layer are linear combinations of the hidden layer neuron outputs as:

$$y_k = \sum_{i=1}^{H} w_{ki} q_i - \theta_k \quad (k = 1, 2, ..., M) \tag{5.3}$$

where w_{ki} is the connecting weights from the i^{th} hidden layer neuron to the k^{th} output layer, θ_k is the threshold value of the k^{th} output layer neuron.

5.3.3 Kriging

The kriging method was developed by the French mathematician Georges Matheron based on the Master′s thesis of Daniel Gerhardus Krige [20], it was first used as a geo statistical method. Sacks et al.[28] firstly introduced Kriging method as a surrogate modeling method, in the paper of Sacks et al.[28], Kriging surrogate model was also called

design and analysis of computer experiment (DACE). The *Kriging* model is a combination of two components [26]: deterministic functions and localized deviations.

$$Y(x) = \sum_{i=1}^{k} f_i(x)\beta_i + z(x) \tag{5.4}$$

where $\sum_{i=1}^{k} f_i(x)\beta_i$ is the term of deterministic functions, β are coefficients of deterministic functions, fi(x) are k known regression functions, which are usually polynomial functions. z(x) is term of localized deviations with mean zero, variance σ^2, and covariance expressed as:

$$Cov[z(x_i), z(x_j)] = \sigma^2 R(x_i, x_j) \tag{5.5}$$

where $R(x_i, x_j)$ is the correlation function between any two of the ns samples The common types of correlation functions are linear function, exponential function, Gauss function, spline function, etc. (Ryu et al. 2002). The prediction of un sampled points response y(x) can be expressed as:

$$\hat{y}(x) = f(x)^T\beta + r^T R^{-1}(Y - F\beta) \tag{5.6}$$

where Y is the vector of ns samples response, r is the correlation vector between samples and prediction points.

$$r = [R(x, x_1), R(x, x_1), ..., R(x, x_1)]^T \tag{5.7}$$

$$F = [f(x_1), f(x_2), ...f(x_{n_x})]^T. \tag{5.8}$$

5.4 Toolbox used for different surrogate models

Table 5.1 details the different surrogates used during this investigation. The SURROGATES toolbox was also used for easy manipulation of the surrogates.

Table 5.1: Setup for the set of used surrogates. The DACE [18], RBF[14] and SURROGATES [31] toolboxes were used to run the kriging, radial basis function and polynomial response surface respectively.

Table 5.1: Different surrogates used during this investigation

Surrogate	Details
KRG	Kriging model: constant trend function and Gaussian correlation
PRS	Polynomial response surface: Second degree polynomial
RBF	Radial basis function: Multiquadric basis function

5.5 Test Function for Kriging Surrogate Model

The Himmelblau function is taken as a test function. It has one local maxima and four local minima in the domain x = [-6,6] and y = [-6,6]. The function is defined as

$$f(x, y) = (x^2 + y - 11)^2 + (x + y^2 - 7)^2 \tag{5.9}$$

$$x \in [-6, 6]; \quad y \in [-6, 6] \tag{5.10}$$

It has one local maximum at x=-0.270845 and y=-0.923039 where f(x,y)=181.617, and four identical local minima:

$$f(3.0000, 2.0000) = 0.0 \tag{5.11}$$

$$f(-2.8051, 3.1313) = 0.0 \tag{5.12}$$

$$f(-3.7793, -3.2831) = 0.0 \tag{5.13}$$

$$f(3.5844, -1.8481) = 0.0 \tag{5.14}$$

$$\tag{5.15}$$

If a small number of design points are used to create a surrogate model, then the approximate model created is prone to large errors at the trial points. However, the prediction accuracy of a surrogate model cannot be improved merely by taking larger number of design points; that is a function of its behaviour, design space and the required accuracy. Fig. 5.5 shows the effect of increase in number of design points on the Root Mean Square Error (RMSE) of this test function. It is seen that the prediction accuracy of the model improves till 120 design points, after which addition of more design points does not approximate model for surrogate on the right with all the design points and test points. The actual value fo the function and predicted value from the surrogate model at test points are seen to match with each other within 1%.

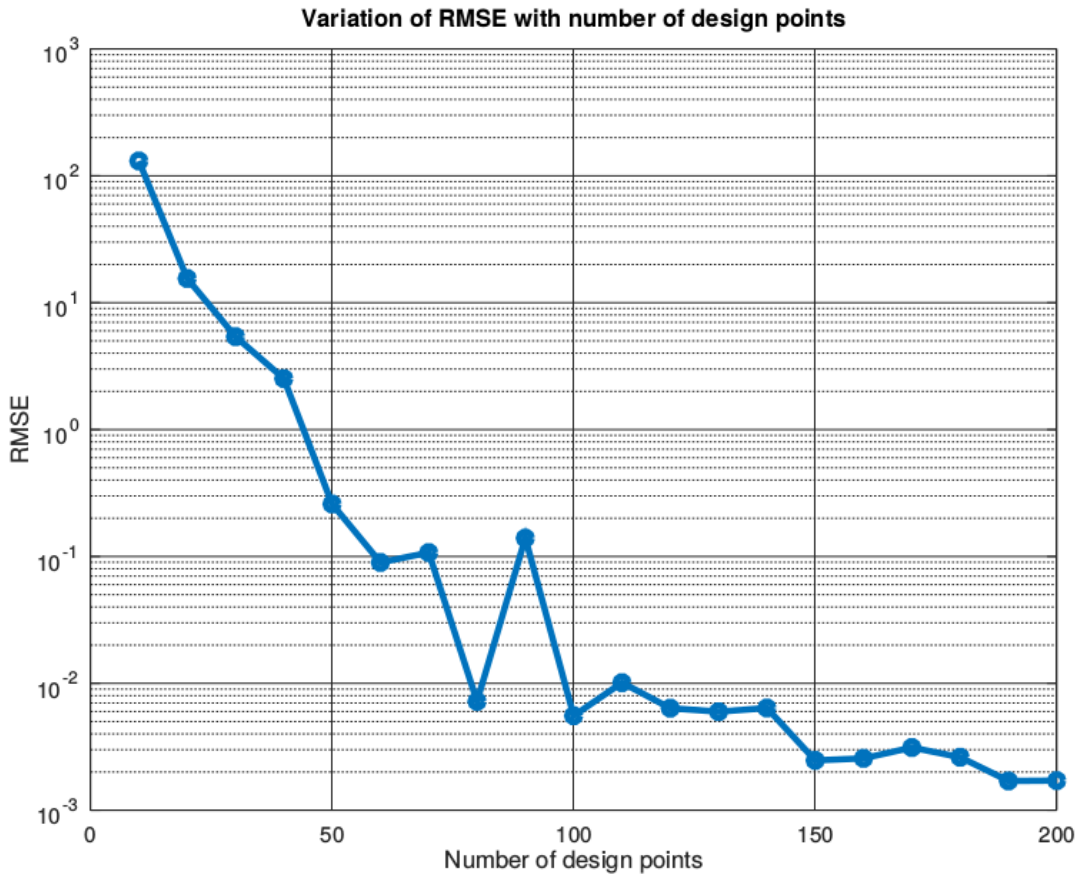

Figure 5.5: Root Mean Square Error with Design Points considered

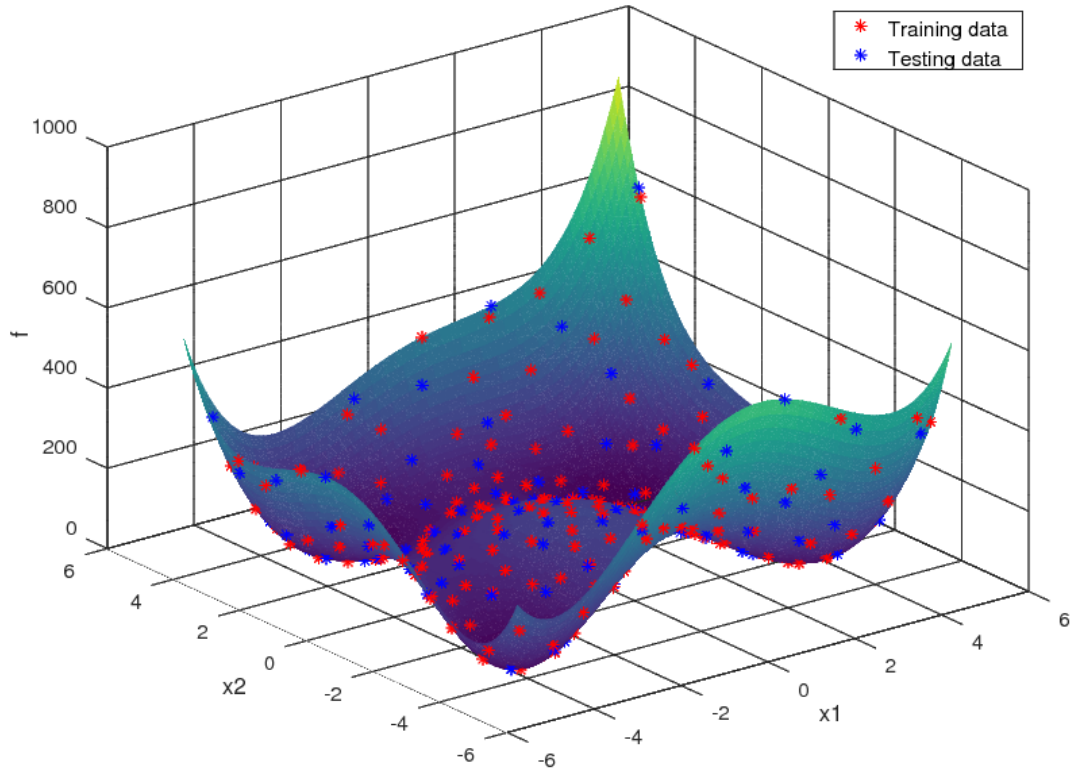

Figure 5.6: Comparison of Himmelblau function with its Surrogate Model

5.6 Coupling of Genetic Algorithm, Surrogate model and testing for modified Himmelblau functions

It is a well known fact that evolutionary algorithms like Genetic algorithm searches for global minimum and outputs that global minimum as final answer. Unlike gradient based methods, it should not get struck in local minimum. In order to check this, we modify the existing Himmelblau function. This is because actual Himmelblau function has four identical local minimum and don't have any global mimima. So, we modify it by adding the term $0.01 * (x + 3.7793)^2 + (y + 3.2832)^2$. This term is added to the function value evaluated at all points except (-3.7793,-3.2832). Hence we obtained modified Himmelblau function with one global minima at (-3.7793,-3.2832) and three local minima at other three points. If we optimise this modified Himmelblau function using Genetic algorithm, we have to get the final answer as (-3.7793,-3.2832). The same answer is expected using surrogate model for the modified Himmelblau function. The obtained results are shown in Table 5.3

The genetic algorithm code used is a MATLAB code is written by Xavier [22]. The input parameters used are default values given by author and are specified in Table 5.2. NVAR is the number of variables (2 for present case).

Table 5.2: Genetic algorithm parameters

Parameter	Value
Population size	NVAR*50
Crossover probability	0.9
Mutation probability	0.1
Number of generation	NVAR*20+10
Selection scheme	Roulette wheel selection method

Table 5.3: Results obtained for modified Himmelblau function

	X	Y	Function value
Actual Function	-3.7793	-3.2832	1.6725e-11
Surrogate model	-3.7791	-3.2828	2.5643e-03
% error	0.006	0.013	NA

To explain the query of what happends if we take less number of design points while fitting the surrogate model, consider modified Himmelblau function discussed in Section 5.6. From Fig. 5.5, we can infer that we need at least 150 design points to get develop a surrogate model which mimics actual Himmelblau function. But instead of 150 points, lets take only 20 points and construct a Kriging surrogate model and find the optimal point. It is already known that the optimal points is (-3.7793,-3.2872). If we couple the genetic algorithm optimizer with surrogate model developed using only 20 points, we get the following results.

Table 5.4: Results obtained for 20 design points

	X	Y	Function value
Actual Function	-3.7793	-3.2832	1.3278e-13
Surrogate model	-3.2205	-2.9549	-6.3131
% error	14.79	10.00	NA

From the above table we may see that if the number of design points used to train the model are low and if this model is coupled with optimizer, we end up getting sub-optimal solution with some percentage error.

Chapter 6

Surrogate model for CFD

To develop a surrogate model which mimics the behaviour of CFD in finding the drag coefficient at zero degree angle of attack, it is essential to identify the limits of design parameters, perform Design Of Experiments (DOE) on them, perform CFD analysis at these DOE points and fit a surrogate model. The whole processes is described in the subsections below.

6.1 Mapping design variables

The first task before creation of DOE was the proper definition of the upper and lower limits for the six design variables (viz., $m, r_0, r_1, C_p, \frac{l}{d}$ *and scale_y*). The upper and lower limits of design variables are calculated using the initial sizing done by Alam [2]. The design space is confined as mentioned in Table 6.1

Table 6.1: Design Space

Design Parameters	Min.	Max.
$Point\ of\ Max.\ Dia., m$	0.35	0.50
$Nose\ Radius, r_o$	0.20	0.80
$Tail\ Radius, r_1$	0.1	0.5
$Prismatic\ Coeff., C_p$	0.55	0.70
$Fineness\ Ratio, \frac{l}{d}$	2.50	6.00
$Scaling\ in\ Y\ direction,\ scale\_y$	1.00	3.00

Eighty candidate points were first obtained by Surrogates Toolbox **cite surrogate toolbox** using the Optimal Latin Hypercube Sampling (OLHS) method. The generated points were then mapped to the shapes corresponding to envelope having *Reynolds number (Re)* of 3.01e6.

6.2 Design of Experiments study

As mentioned previously in Section 5.2, DOE study is used to extract maximum amount of information from every experiment conducted. This is especially needed when we are carrying out expensive computer or real life experiments. While developing surrogate model for CFD, each CFD analysis will take about 3 hours to complete. Hence to optimally use the computation resources, the total number experiments needs to be as low as possible but extracting maximum information about function behaviour. So, initially the number of experiments are taken as 80 and the design points are generated using the *Optimal Latin Hypercube Sampling (OLHS)* technique present in SURROGATES Toolbox by Viana [32]. The obtained points are given in Appendix.

6.3 Training data for CFD surrogate model

All the pre-processing required to perform CFD analysis like creating geometry, deciding grid size and meshing the domain has been automated using Octave and C++ scripting. In our case, 80 DOEs are generated and steady state 3D CFD analysis has been performed for these 80 shapes. The solver parameters used are as follows:

Table 6.2: Flow conditions and solver parameters for all DOE shapes

Parameters	Value
Reynolds number based on volume Re	$3.01 * 10^6$
Pressure, (N/m^2)	87500
Density, (Kg/m^3)	1.057
Speed, (m/s)	51
Mesh	Hexahedral mesh using *blockMesh* and *snappyHexMesh*
Solver	*SimpleFOAM* (Incompressible steady state solver)
Turbulent..?	Yes
Turbulence model	K-Omega SST

6.4 Grid Convergence study

Effect of grid size on the overall results by changing the number of cells in self similar mesh has been carried out. Below is the plot of variation of pressure and viscous drag with number of cells for a simulation. As mentioned by Suman et al.[30] , when the percentage change in the values is less than 5 %, then the solution is reported to have grid convergence.

Table 6.3: Grid convergence study

Cells	Pressure Drag (N)	Viscous Drag (N)
376380	1.1	11.02
604375	2.2	11.68
840565	2.02	12.1
994864	2.09	12.24
1563471	2.12	12.5

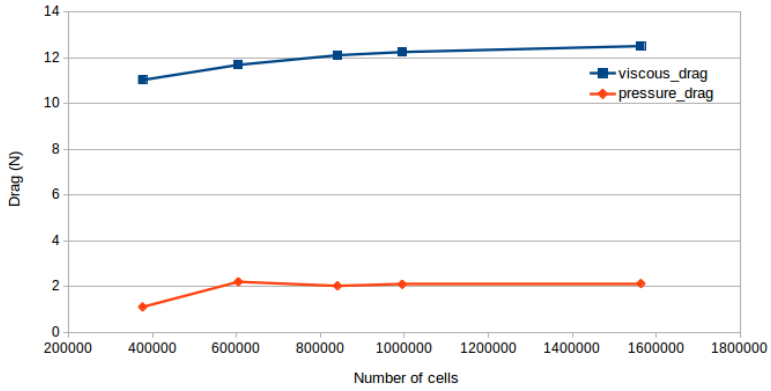

Figure 6.1: Variation of pressure and viscous drag with number of cells

Since there is no considerable amount of change in drag values, the number of cells are taken are around 1 million instead of 1.5 million for all the cases. This saves computational time.

6.5 Results of CFD simulations

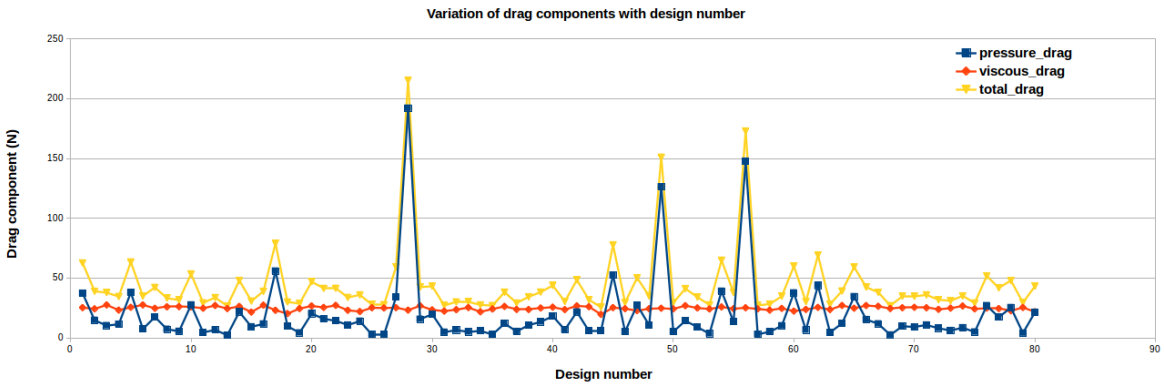

Figure 6.2: Variation of pressure and viscous drag with design number

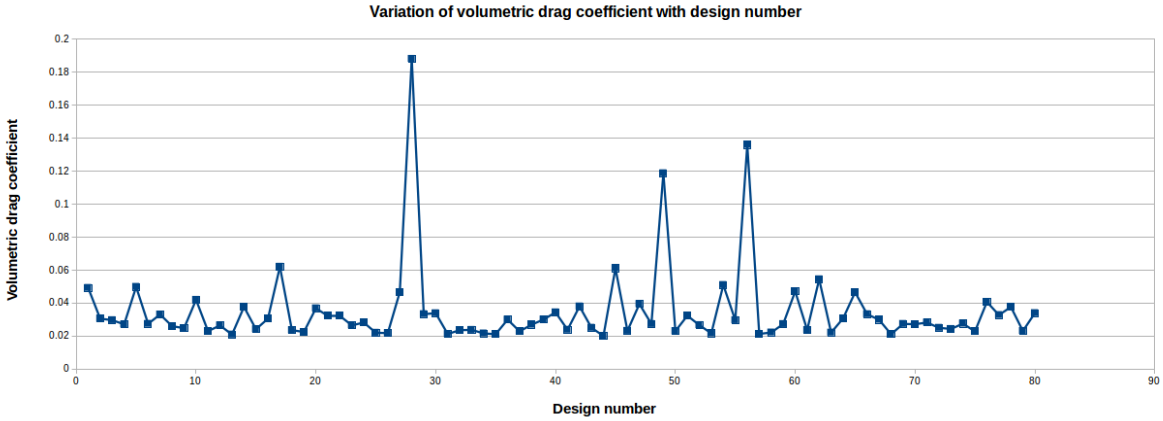

Figure 6.3: Variation of volumetric drag coefficient with design number

From Fig. 6.3 we can see that some shapes are having very high drag coefficient compared to others. To see one of these high and low drag bodies visually, they have been drawn in Fig. 6.4 one on top of other with scale being the same. Given a fixed volume, bodies with non-axisymmetric shapes will have higher frontal area compared to axisymmetric body as shown in Fig.6.4. This makes the non-axisymmetric body more 'bluffy'. This leads to flow separation which is a non-linear phenomenon.

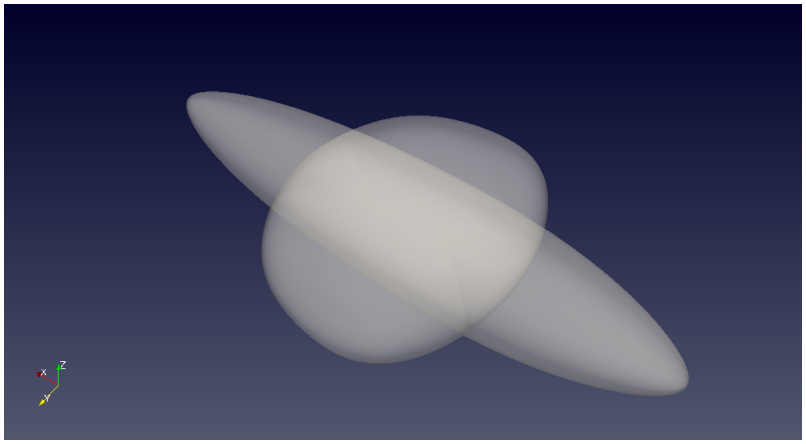

Figure 6.4: Visual comparison of low and high drag bodies

The surface streamlines have been plotted in Figure 6.5 and 6.6 to understand the physics behind large difference in drag. It can be seen that long sleek body is having very less flow separation at the leading edge whereas the other body with more frontal area is have more flow separation and wake region.

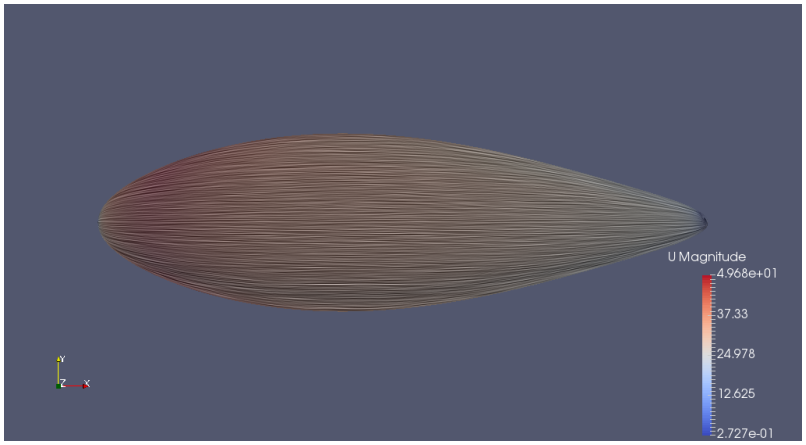

Figure 6.5: Surface streamlines on the body with low pressure drag

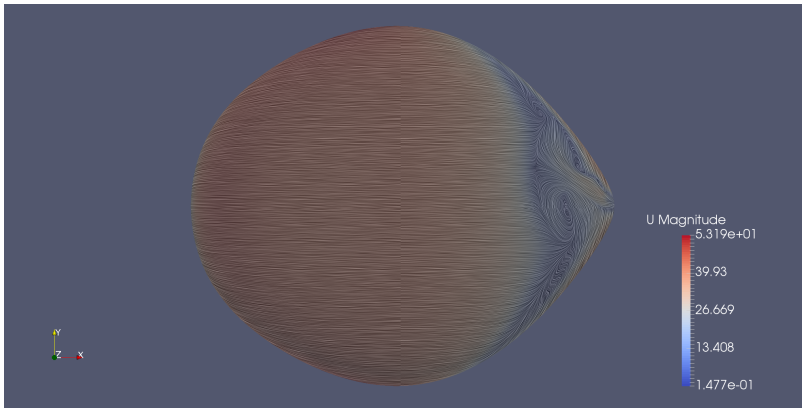

Figure 6.6: Surface streamlines on the body with high pressure drag

To couple a surrogate model with optimizer, the model needs to be accurate enough. The % error should be less than 2% as suggested by Alam[2]. But because of large variance in the training data, the model obtained is not accurate enough. This is because the bodies having more pressure drag because of flow separation are acting as outliers in the training data. So, the bodies having volumetric drag coefficient more than 0.04 are not considered while fitting the model. This gives a fairly better model with % error $\leq 6\%$ in the case of Kriging. Since the few bodies with higher drag are acting as outliers for the model, they are not considered while training the model. So, bodies with $C_{DV} \geq 0.04$ are not considered in model building. To improve the accuracy of model, 40 more points are added to training set.

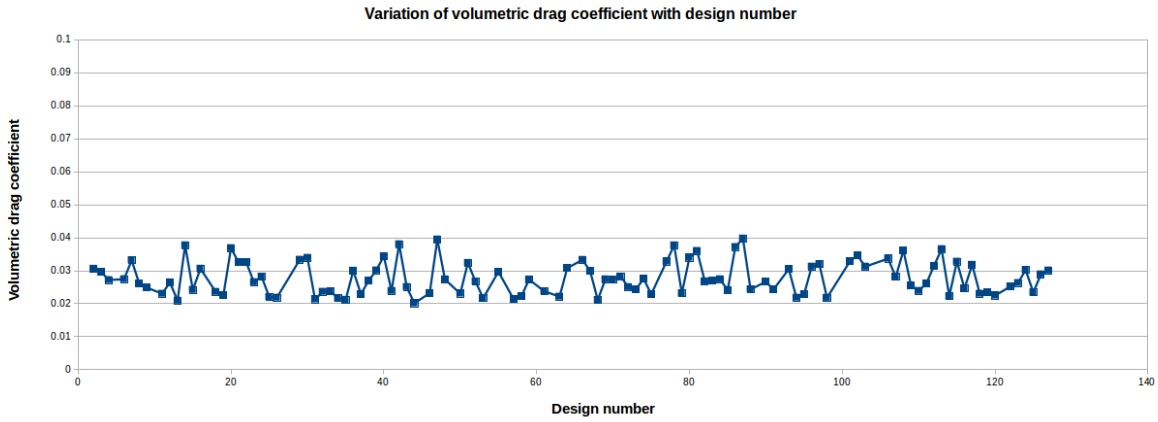

Figure 6.7: Variation of volumetric drag coefficient with design number for training dataset

6.6 Testing the accuracy of surrogate model

Three surrogate models mentioned in Section 5.1 has been fit to the above data. Then eight random design points has been generated in the domain for testing purpose. The results are shown in Table 6.4.

Table 6.4: Accuracy of different surrogate models

Random Exp.No	Kriging (% Error)	PRS (% Error)	RBF (% Error)
1	5.72	3.24	2.73
2	4.82	11.33	36.40
3	0.96	6.09	12.73
4	1.15	7.98	18.62
5	2.50	5.40	14.13
6	1.29	6.31	1.75
7	1.99	0.59	10.05
8	5.64	3.36	1.12
Avg. % Error	3.00875	5.5375	12.19

From the above results we can observe that Kriging predicted the functional behaviour with more accuracy. RBF is having more error because the amount of training data to fit RBF is not sufficient in our case. Accuracy of polynomial response surface is between Kriging and Radial basis function. This is because PRS only sees at the global

functional behaviour and under-fits the model. So, Kriging has been selected for coupling with optimizer in our study.

Also, few machine learning algorithms have been applied to see if they predict better than Kriging. It can be seen from Table 6.5 that none of them is predicting the functional behaviour better than Kriging. The reason is obvious as machine learning models are very generalized models and they can be used for both numerical and non-numerical experiments provided that large amount of training data is available. Since in our case the data is limited, we cannot use machine learning models. This further demonstrates the efficacy of Kriging for predicting functional behaviour of numerical experiments.

Table 6.5: Accuracy of different machine learning models

Random Exp.No	Linear Regression (% Error)	Ridge Regression (% Error)	SVR (% Error)	Kernel Ridge (% Error)
1	4.89	8.45	48.86	37.40
2	22.60	31.31	74.30	96.77
3	31.62	33.77	77.00	115.31
4	20.15	24.09	74.03	96.03
5	15.34	16.81	45.69	59.07
6	11.67	1.08	27.72	21.22
7	12.90	15.42	48.52	62.18
8	1.68	17.80	64.92	62.44
Avg. % Error	15.10	18.59	57.63	68.80

Chapter 7

Calculation of Hoop Stress

In order to maintain positive pressure inside the envelope, three main loadings are considered to estimate the internal over pressure (ΔP) viz., the loading due to dynamic pressure, aerodynamic loading, and hydro-static pressure as suggested by Gupta & Malik [12] . A brief description of these three components of the module is as given below.

Dynamic Pressure: Dynamic pressure loading acts on the front portion of the aerostat envelope and tries to make a depression on the envelope surface, its diameter depends on the region of highly stressed area which is normally 7 to 9 % of the envelope length. To maintain the shape of the envelope, the internal pressure is kept slightly higher than dynamic pressure, normally 15% as suggested by Gupta & Malik [12] as per Eq. 7.1

$$\Delta P_{dyn} = 1.15\left(\frac{1}{2}\rho_{air}v^2\right) \tag{7.1}$$

Aerodynamic Pressure: Aerodynamic pressure loading results from applying the stability conditions to the airship. Coefficient of pressure, as observed normally for airship profiles is in the range of 0.30 to 0.35 from the leading edge, but normally for such shapes, it is assumed at the maximum diameter. is used for calculating the pressure due to this loading.

$$\Delta P_{aer} = c_p\left(\frac{1}{2}\rho_{air}v^2\right) \tag{7.2}$$

Hydrostatic Pressure: Hydrostatic pressure loading is due to the difference between the height of the top and bottom of aerostat and could be quite substantial of the aerostat diameter in large. The hydrostatic pressure as observed at mean centerline axis of the envelope is calculated at maximum diameter using:

$$\Delta P_{hyd} = \frac{1}{2}(\rho_{air} - \rho_{He})gD_c \tag{7.3}$$

The sum of pressure due to these three loadings gives the total required internal pressure. Since the aerostat envelope diameter is more than twenty times of the thickness of the material; it can be considered as a very thin shell and hence hoop stress is calculated in terms of the circumferential unit load as shown in Eq. 7.4

$$\Delta P = \Delta P_{dyn} + \Delta P_{aer} + \Delta P_{hyd} \tag{7.4}$$

To estimate the longitudinal stress (σ_l) and the circumferential hoop stress (σ_h) developed in an envelope, an equivalent cylindrical envelope is considered, having the same surface area and volume as the actual airship envelope, as shown in Fig 7.1

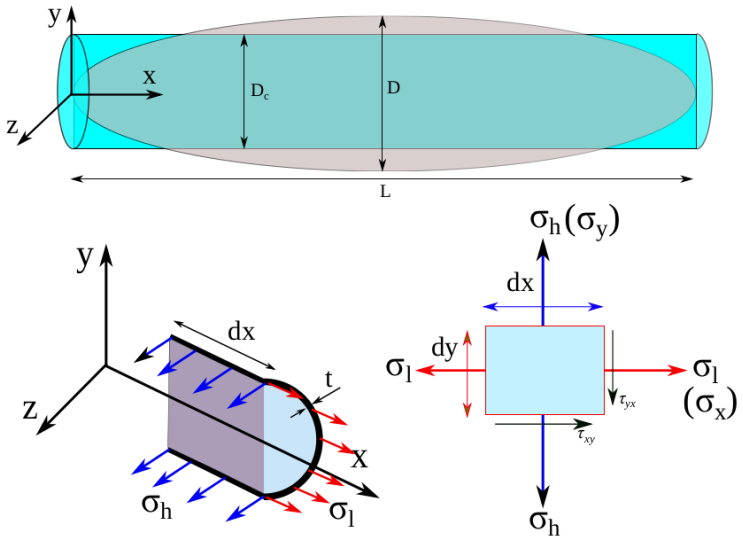

Figure 7.1: Stress representation in envelope 2

Hence, σ_l and σ_h developed in an envelope are estimated as:

$$\sigma_h = \frac{\Delta P D_c}{2} \tag{7.5}$$

$$\sigma_l = \frac{\Delta P D_c}{4} \tag{7.6}$$

To maintain the aerodynamic shape and rigidity of an airship envelope some pressure difference ($\Delta P^{'}$) is also needed, which can be determined by bending moment estimation.

7.0.1 Bending Moment Calculation

An empirical relation for maximum bending moment given by FAA 5 can be expressed as:

$$M = 0.029[1 + (f - 4)(0.5624L^{0.02} - 0.5)]\, \rho_{air}.u.v.V_{env}L^{0.25} \tag{7.7}$$

Where D, is the diameter of airship envelope with the where u and v are the gust and wind velocity respectively. Eq. 7.7 is valid for fineness ration between 4 to 6. For fineness ratio less than 4, f can be assumed as 4. The point at which the maximum bending moment occurs, i.e., near the center of gravity, σ_l at the top of this must be greater than or equal to zero. Therefore, the equation for σ_l can be written as:

$$\sigma_l = \frac{\Delta P^{'} \pi R^2}{2\pi R} - \frac{MRT}{I} \geq 0 \tag{7.8}$$

Where R is the radius of airship envelope at the point of maximum bending. t is the thickness the envelope material. I is the second moment of area, which has the value of $\pi R^3 t$. Minimum pressure required $\Delta P^{'}$ to maintain the shape of the envelope can be calculated as:

$$\Delta P^{'} = \frac{16M}{\pi D^3} \tag{7.9}$$

Where D is the diameter of airship envelope with the assumption that, the location of maximum bending is same as the location of maximum diameter. Total differential pressure âĹĘP t can be obtained as:

$$\Delta P_t = max(\Delta P, \Delta P^{'}) \tag{7.10}$$

In that case, σ_h and σ_l can be calculated as:

$$\sigma_h = \frac{\Delta P D_c}{2} \tag{7.11}$$

$$\sigma_l = \frac{\Delta P D}{4} + \frac{4M}{\pi D^2} \tag{7.12}$$

von-Mises Stress Calculation: From the principle stresses, von-Mises stress can be expressed as:

$$\sigma_v = \left[\frac{(\sigma_1 - \sigma_2)^2 + (\sigma_2 - \sigma_3)^2 + (\sigma_3 - \sigma_1)^2}{2} \right]^{\frac{1}{2}} \tag{7.13}$$

Stresses are considered only in 2-D planes due to very low thickness of envelope compared to its diameter. Therefore $\sigma_3 = 0$, which simplifies the equation as:

$$\sigma_v = \sqrt{\frac{(\sigma_1 - \sigma_2)^2 + \sigma_1^2 + \sigma_2^2}{2}} \tag{7.14}$$

$$\sigma_v = \sqrt{\sigma_1^2 + \sigma_2^2 - \sigma_1 \sigma_2} \tag{7.15}$$

Chapter 8

Results and discussion

8.1 Optimal results case 1

Table 8.1 shows the design parameters of the optimal shape with minimum aerodynamic drag. It can be observed that the $scale_y$ parameter is 1 which means the optimal shape is axisymmetric. The results is obvious as given a fixed volume, axisymmetric bodies will have minimum frontal area which is responsible for pressure drag. The shape is shown in Fig. 8.1

Table 8.1: Optimal solution obtained for minimum C_{DV} case 1

Design Parameters	Optimal value for minimum C_{DV}
$Point\ of\ Max.\ Dia., m$	0.40910
$Nose\ Radius, r_o$	0.8
$Tail\ Radius, r_1$	0.30428
$Prismatic\ Coeff., C_p$	0.61521
$Fineness\ Ratio, \frac{l}{d}$	5.69420
$Scaling\ in\ Y\ direction,\ scale\_y$	1
$Kriging\ C_{DV}$	0.01796181
$von-Mises\ stress\ \sigma_v\ (Pa)$	403.47

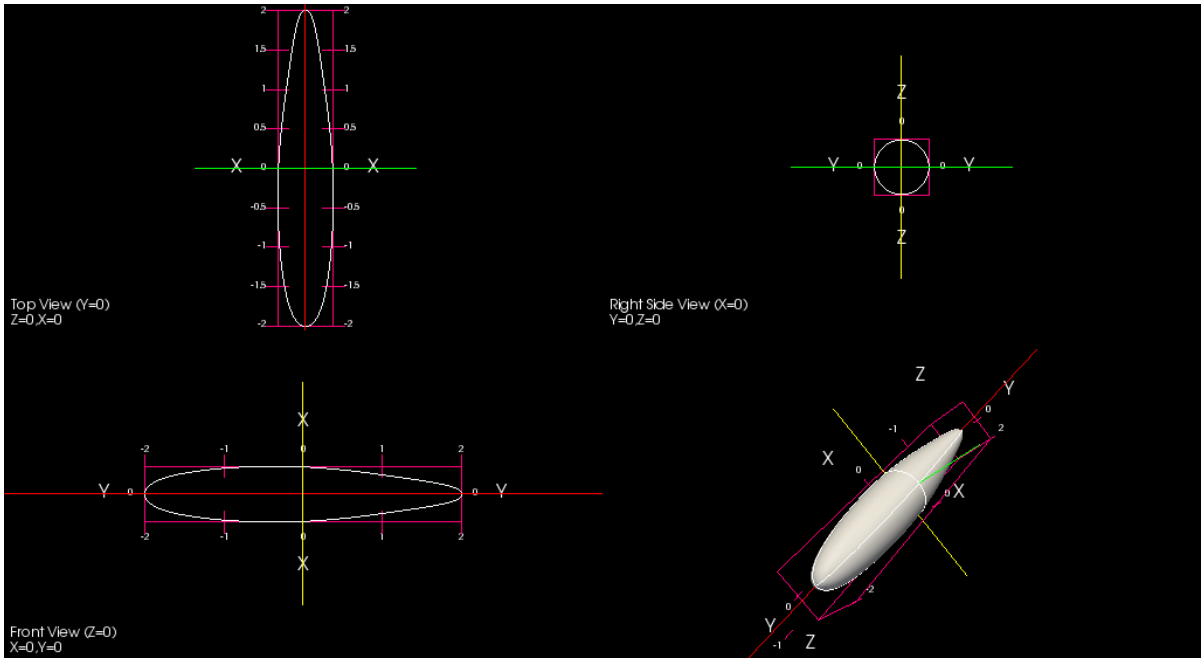

Figure 8.1: Optimal shape obtained for minimum C_{DV} case 1

8.2 Composite objective function

Two disciplines namely aerodynamics and structures which involves the calculation of aerodynamic drag (C_{DV}) and von-Mises (σ_v) stress are considered for shape optimization of airship profile. The aim is to have lowest possible aerodynamic drag and von-Mises stress. To achieve this, we need a composite objective function minimizing which, both C_{DV} and σ_v are minimized simultaneously. The composite objective function can be written as

$$F_{comp} = \frac{1}{2}\left(\frac{C_{DV}}{C_{DV,ref}} + \frac{\sigma_v}{\sigma_{v,ref}}\right) \tag{8.1}$$

Where, $C_{DV,ref}, \sigma_{v,ref}$ are the values of these parameters corresponding to the reference shape. The values obtained for minimum C_{DV} and $\sigma_{v,ref}$ in Table 8.1 are taken as reference values for $C_{DV,ref}$ and $\sigma_{v,ref}$ respectively. The composite objective function now becomes:

$$F_{comp} = 0.5 * (55.67 * C_{DV} + 2.607e - 3 * \sigma_v) \tag{8.2}$$

Since the bodies with $C_{DV} \geq 0.04$ are not considered while developing the surrogate model, it cannot predict shapes with $C_{DV} \geq 0.04$ with much confidence. So, F_{comp} has been modified with penalty function i.e when the optimizer is considering a shape with $C_{DV} \geq 0.04$, we give huge penalty so that it wont go beyond 0.04. the Table 8.2 shows the

optimal results obtained by minimizing Eqn. 8.2 using genetic algorithm. The parameters of shape obtained are shown in Table 8.2.

Table 8.2: Optimal solution obtained for minimum F_{comp} case 1

Design Parameters	Optimal value for minimum F_{comp}
$Point\ of\ Max.\ Dia., m$	0.40942
$Nose\ Radius, r_o$	0.79999
$Tail\ Radius, r_1$	0.30606
$Prismatic\ Coeff., C_p$	0.61508
$Fineness\ Ratio, \frac{l}{d}$	5.75445
$Scaling\ in\ Y\ direction,\ scale\_y$	1
$Kriging\ C_{DV}$	0.018116
$von-Mises\ stress\ \sigma_v\ (Pa)$	402.47
F_{comp}	0.99941

8.3 Optimal results case 2

To obtain optimal shapes for non-axisymmetric shapes, the lower limits of $Scale_y$ in genetic algorithm is changed from 1 to 2 i.e we are deceasing the size of design space and forcing the optimizer not to reach an axisymmetric shape. This is particularly useful when we have constraint on the curvature of envelope. The parameters of optimal shape obtained are shown in Table 8.3. This shows that the drag has increased by 17.15 %. The shape is shown in Fig.8.2

Table 8.3: Optimal non-axisymmetric envelope obtained for minimum C_{DV} case 2

Design Parameters	Optimal value for minimum C_{DV}
$Point\ of\ Max.\ Dia., m$	0.37201
$Nose\ Radius, r_o$	0.62891
$Tail\ Radius, r_1$	0.15214
$Prismatic\ Coeff., C_p$	0.64283
$Fineness\ Ratio, \frac{l}{d}$	5.53748
$Scaling\ in\ Y\ direction,\ scale\_y$	2.00000
$Kriging\ C_{DV}$	0.02064
$von-Mises\ stress\ \sigma_v\ (Pa)$	415.29

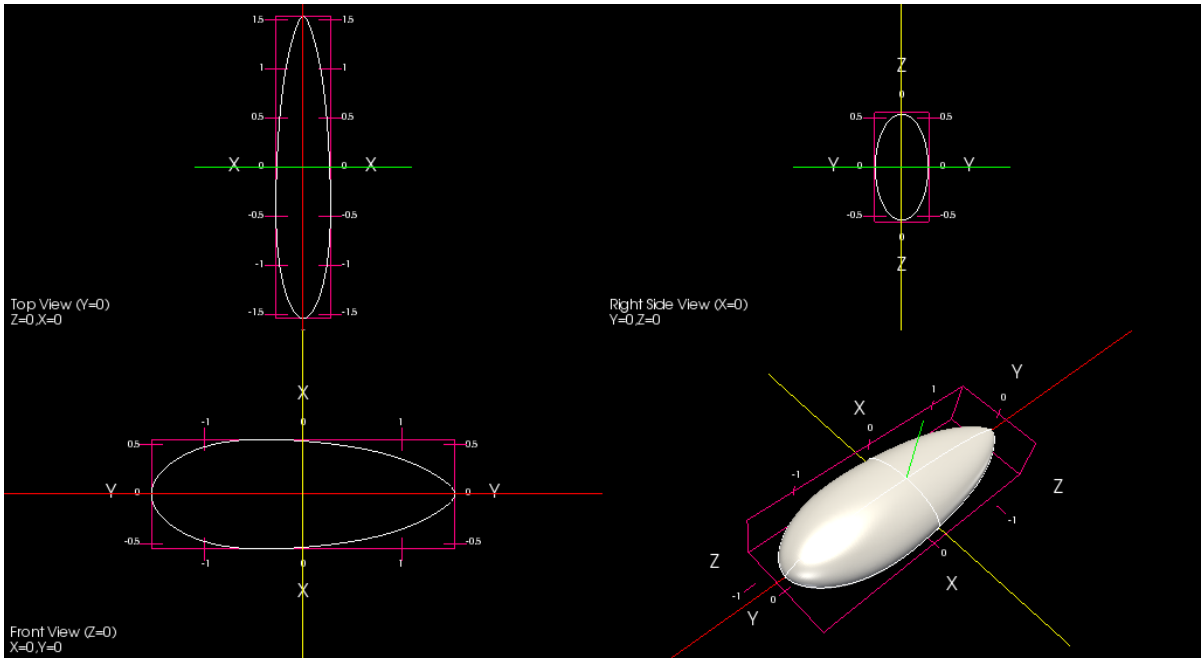

Figure 8.2: Optimal non-axisymmetric shape obtained for minimum C_{DV} case 2

$$F_{comp} = \frac{1}{2}\left(\frac{C_{DV}}{C_{DV,ref}} + \frac{\sigma_v}{\sigma_{v,ref}}\right) \tag{8.3}$$

The values of C_{DV} and σ_v from Table 8.3 are taken as reference values for $C_{DV,ref}$ and $\sigma_{v,ref}$ respectively. The composite objective function now becomes:

$$F_{comp} = 0.5 * (48.4496 * C_{DV} + 2.4079e - 3 * \sigma_v) \tag{8.4}$$

Table 8.4: Optimal non-axisymmetric envelope obtained for minimum F_{comp} case 2

Design Parameters	Optimal value for minimum F_{comp}
$Point\ of\ Max.\ Dia., m$	0.37207
$Nose\ Radius, r_o$	0.62949
$Tail\ Radius, r_1$	0.15479
$Prismatic\ Coeff., C_p$	0.64237
$Fineness\ Ratio, \frac{l}{d}$	5.63750
$Scaling\ in\ Y\ direction,\ scale\_y$	2.00000
$Kriging\ C_{DV}$	0.020687
$von-Mises\ stress\ \sigma_v\ (Pa)$	413.52
F_{comp}	0.99900

8.4 Optimal results case 3

If we further change the lower limits of the genetic algorithm optimizer from 2 to 2.5, we obtain the following shape. Here the percentage increase in drag is

Table 8.5: Optimal non-axisymmetric envelope obtained for minimum C_{DV} case 3

Design Parameters	Optimal value for minimum C_{DV}
$Point\ of\ Max.\ Dia., m$	0.47998
$Nose\ Radius, r_o$	0.74580
$Tail\ Radius, r_1$	0.17931
$Prismatic\ Coeff., C_p$	0.66849
$Fineness\ Ratio, \frac{l}{d}$	5.81668
$Scaling\ in\ Y\ direction,\ scale\_y$	2.58996
$Kriging\ C_{DV}$	0.022040
$von-Mises\ stress\ \sigma_v\ (Pa)$	401.01

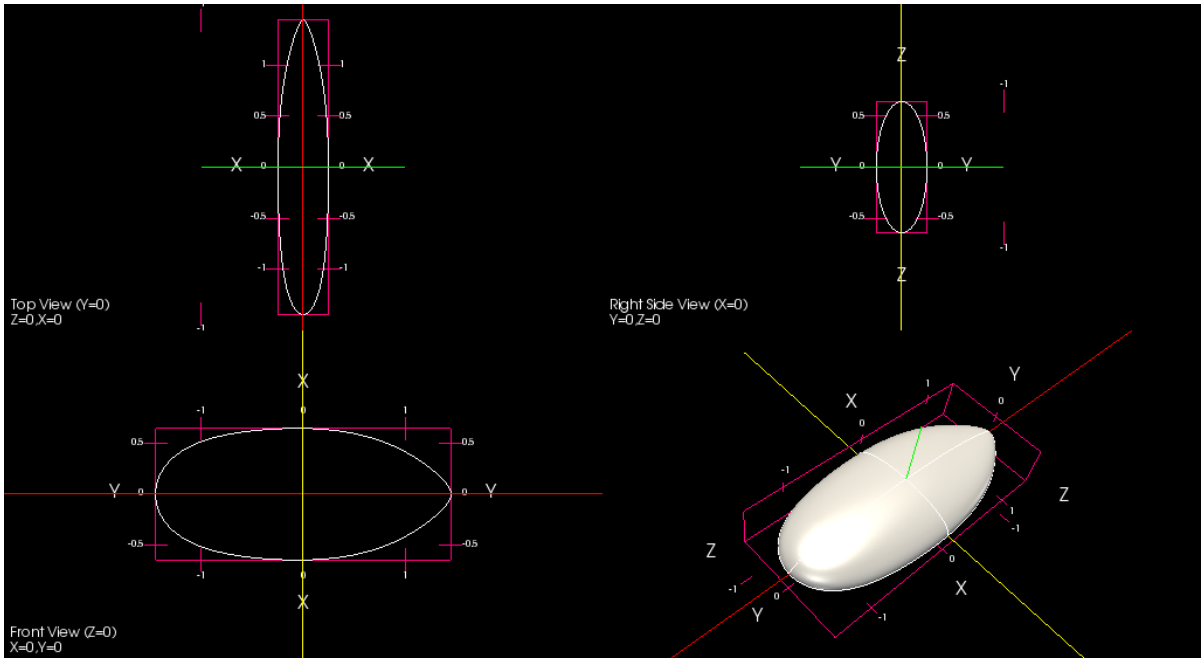

Figure 8.3: Optimal non-axisymmetric shape obtained for minimum C_{DV} case 3

Chapter 9

Conclusions, Limitations and Future Work

In the present study, a methodology for optimization of non-axisymmetric shapes has been developed. The same methodology can be used for the optimization of non-axisymmetric shaped submarines, hybrid airships and stratospheric airships with solar panels installed on the top side. The methodology parameterizes the envelope geometry, creates the geometrical shape and solves for drag using surrogate model. This surrogate model can be coupled as an alternate to CFD to find zero lift drag without having the need to run CFD every time in optimization routine. This helps the designer to find better shapes using non-axisymmetric envelopes as he/she has more design space for exploration compared to axisymmetric shapes.

9.1 Observations & Conclusions

OpenFOAM software with its meshing, solving and post-processing capabilities are very helpful in performing 3D CFD analysis. The automatic mesh generation utility is found to be very helpful in automating the processes of optimization.

The envelope geometry parameterization algorithm has found to be very efficient in capturing all the standard axisymmetric shapes [2] available in literature along with non-axisymmetric shapes given by Ceruti et al.[4]

Kriging based surrogate models are found to be better in predicting the functional behaviour of numerical experiments. Kriging is even better than state of the art machine learning models. However the average accuracy is 3 % with maximum percentage error being 6%. This can be further improved by considering more number of points in Design

Of Experiments (DOE) study. But because of time constraints, the 3% accurate model has been coupled with optimizer.

It has been observed that axisymmetric shapes are better for drag reduction however forcing the shape to be non-axisymmetric, the drag has been increased by 14.92 %. This is particularly advantages when the percentage increase in other performance parameters like solar irradiation is very high for compromise of 14.92 % increase in drag.

9.2 Limitations of the present study

The present study is limited to do only steady state CFD simulations for non-separating flows. However to study the effect of flow separation on bluff bodies like airships, unsteady CFD analysis has to be carried out. More accurate method is to consider aeroelastic effects on the drag. Moreover all the numbers for drag in present study are within 3%.

9.3 Future work

It would be interesting to know the percentage increase in solar irradiation when the envelope gets flatter upper surface. The trade off between solar irradiation and drag can be studied. The envelope geometry parameterization can further be modified to capture cambered and multi lobe bodies which is very useful for hybrid airships and submarines.

Appendix

Table 1: Table of design points obtained from OLHS

Exp.No	m	r0	r1	cp	L by D	$Scale_y$
1.0000	0.4677	0.2000	0.3734	0.6829	3.5190	2.0886
2.0000	0.4165	0.4582	0.4190	0.5956	3.0759	1.8861
3.0000	0.4753	0.6101	0.2468	0.6354	4.8481	2.9241
4.0000	0.3576	0.7241	0.4392	0.6411	2.8987	1.4051
5.0000	0.4259	0.5494	0.1911	0.6981	3.4747	2.2911
6.0000	0.4278	0.2456	0.1709	0.5595	5.3354	2.7975
7.0000	0.4924	0.5342	0.3430	0.6241	3.3861	1.9367
8.0000	0.4127	0.4886	0.4089	0.5747	5.8671	2.0380
9.0000	0.3842	0.7165	0.2013	0.5690	5.6456	2.5443
10.0000	0.4715	0.4278	0.4899	0.6392	3.7848	2.3671
11.0000	0.4146	0.5266	0.2722	0.5975	5.0253	1.6329
12.0000	0.3557	0.3139	0.1354	0.6013	5.5570	2.7215
13.0000	0.4184	0.7468	0.3177	0.6316	5.2468	1.0759
14.0000	0.4905	0.2835	0.2114	0.6449	4.0949	2.4684
15.0000	0.3728	0.3975	0.3582	0.6146	3.1203	1.1266
16.0000	0.3785	0.5570	0.3633	0.6222	5.1582	2.8987
17.0000	0.4430	0.3443	0.2063	0.6810	2.8101	1.4557
18.0000	0.3747	0.2759	0.3380	0.6582	6.0000	2.8228
19.0000	0.4241	0.6861	0.5000	0.6772	4.7595	1.0506
20.0000	0.4886	0.5038	0.3532	0.6905	4.5823	2.5190
21.0000	0.3880	0.3291	0.4443	0.6259	3.8734	2.1899
22.0000	0.4734	0.4734	0.4038	0.5880	5.1139	3.0000
23.0000	0.4962	0.6709	0.1405	0.5538	3.2089	1.5570
24.0000	0.4222	0.2380	0.1152	0.6924	4.3165	1.6076
25.0000	0.4013	0.4506	0.1304	0.5671	5.9557	1.7342

26.0000	0.4354	0.4127	0.3076	0.6506	5.7342	1.3291
27.0000	0.4658	0.7848	0.1456	0.6734	3.2975	2.4177
28.0000	0.4468	0.4430	0.3278	0.6962	2.5443	2.1646
29.0000	0.3823	0.7316	0.4544	0.5633	4.7152	2.8734
30.0000	0.4772	0.5949	0.4747	0.5728	2.8544	1.7848
31.0000	0.3652	0.6253	0.1608	0.6601	5.4684	2.0633
32.0000	0.3994	0.5114	0.3228	0.5519	3.9620	1.2532
33.0000	0.4563	0.6405	0.3886	0.6791	5.7785	1.6835
34.0000	0.3918	0.2684	0.3127	0.5500	4.9810	1.7595
35.0000	0.3937	0.3671	0.1861	0.5766	4.4494	1.0000
36.0000	0.4203	0.6481	0.3025	0.6658	4.4937	2.3924
37.0000	0.3595	0.5873	0.2772	0.6487	3.6519	1.0253
38.0000	0.3633	0.3595	0.4797	0.5614	3.8291	1.4304
39.0000	0.4639	0.7013	0.2570	0.5652	3.7405	2.2658
40.0000	0.3614	0.7696	0.2418	0.5842	3.4304	2.6962
41.0000	0.4525	0.3519	0.3684	0.5785	3.6076	1.3797
42.0000	0.4032	0.3367	0.2367	0.6943	4.5380	2.5949
43.0000	0.3899	0.3899	0.2316	0.6203	5.2911	2.2152
44.0000	0.4696	0.2532	0.1000	0.5937	4.1392	1.1013
45.0000	0.4848	0.5190	0.1051	0.6032	2.9430	2.4937
46.0000	0.4316	0.7544	0.3785	0.5709	4.8038	1.7089
47.0000	0.4829	0.5418	0.1557	0.6525	2.5886	1.3038
48.0000	0.4089	0.4658	0.4291	0.6696	4.0063	1.5063
49.0000	0.4373	0.2608	0.2671	0.6639	2.7658	2.6203
50.0000	0.4335	0.5797	0.2620	0.6886	4.2722	1.2278
51.0000	0.4620	0.3747	0.1253	0.5994	4.4051	2.8481
52.0000	0.3861	0.7924	0.2823	0.6563	5.9114	2.6456
53.0000	0.4791	0.5646	0.4241	0.6070	4.9367	1.1772
54.0000	0.3519	0.7089	0.3481	0.6848	3.9177	2.5696
55.0000	0.4070	0.4051	0.2266	0.5557	3.3418	2.0127
56.0000	0.4108	0.6177	0.3937	0.6867	2.5000	2.9494
57.0000	0.3709	0.4962	0.1203	0.6335	4.6709	1.1519
58.0000	0.4867	0.7392	0.1810	0.6715	5.8228	2.7468
59.0000	0.4810	0.2228	0.4494	0.5899	4.0506	1.8101
60.0000	0.4392	0.6937	0.4139	0.6753	2.9873	1.9873
61.0000	0.4297	0.2152	0.2519	0.6278	3.6962	1.2785

62.0000	0.3956	0.5722	0.4949	0.5861	2.6772	2.7722
63.0000	0.4487	0.2987	0.1962	0.6051	5.3797	1.4810
64.0000	0.3500	0.6785	0.4696	0.6468	5.5127	2.6709
65.0000	0.4582	0.4203	0.2975	0.5823	2.7215	2.3165
66.0000	0.3766	0.3823	0.2165	0.5804	4.2278	2.9747
67.0000	0.4051	0.2304	0.3987	0.7000	5.4241	2.2405
68.0000	0.4601	0.6633	0.2215	0.5576	5.6013	1.6582
69.0000	0.3690	0.2076	0.2873	0.6544	4.6266	1.9114
70.0000	0.4411	0.6329	0.4595	0.6165	5.0696	2.1139
71.0000	0.3538	0.4810	0.4342	0.6127	4.8924	1.8354
72.0000	0.4506	0.7772	0.3329	0.6430	3.5633	1.5316
73.0000	0.4544	0.6025	0.1506	0.6108	4.3608	1.8608
74.0000	0.4449	0.3215	0.3835	0.6297	5.2025	2.4430
75.0000	0.4981	0.7620	0.1759	0.6620	4.1835	1.3544
76.0000	0.5000	0.8000	0.4646	0.6184	3.2532	2.3418
77.0000	0.3975	0.6557	0.1101	0.6089	3.1646	2.1392
78.0000	0.3671	0.3063	0.4848	0.6677	2.6329	1.2025
79.0000	0.4943	0.4354	0.2924	0.5918	5.6899	1.9620
80.0000	0.3804	0.2911	0.1658	0.6373	3.0316	1.5823

Table 2: Training data for surrogate model

Exp.	m	r_0	r_1	C_p	$\frac{L}{D}$	$Scale\_y$	$D_p(N)$	$D_v(N)$	C_{DV}
1	0.4677	0.2000	0.3734	0.6829	3.5190	2.0886	7.0380	4.1772	0.0493
2	0.4165	0.4582	0.4190	0.5956	3.0759	1.8861	6.1519	3.7722	0.0306
3	0.4753	0.6101	0.2468	0.6354	4.8481	2.9241	9.6962	5.8481	0.0297
4	0.3576	0.7241	0.4392	0.6411	2.8987	1.4051	5.7975	2.8101	0.0272
5	0.4259	0.5494	0.1911	0.6981	3.4747	2.2911	6.9494	4.5823	0.0499
6	0.4278	0.2456	0.1709	0.5595	5.3354	2.7975	10.6709	5.5949	0.0275
7	0.4924	0.5342	0.3430	0.6241	3.3861	1.9367	6.7722	3.8734	0.0332
8	0.4127	0.4886	0.4089	0.5747	5.8671	2.0380	11.7342	4.0759	0.0261
9	0.3842	0.7165	0.2013	0.5690	5.6456	2.5443	11.2911	5.0886	0.0249
10	0.4715	0.4278	0.4899	0.6392	3.7848	2.3671	7.5696	4.7342	0.0420
11	0.4146	0.5266	0.2722	0.5975	5.0253	1.6329	10.0506	3.2658	0.0230
12	0.3557	0.3139	0.1354	0.6013	5.5570	2.7215	11.1139	5.4430	0.0265
13	0.4184	0.7468	0.3177	0.6316	5.2468	1.0759	10.4937	2.1519	0.0210

14	0.4905	0.2835	0.2114	0.6449	4.0949	2.4684	8.1899	4.9367	0.0377
15	0.3728	0.3975	0.3582	0.6146	3.1203	1.1266	6.2405	2.2532	0.0242
16	0.3785	0.5570	0.3633	0.6222	5.1582	2.8987	10.3165	5.7975	0.0306
17	0.4430	0.3443	0.2063	0.6810	2.8101	1.4557	5.6203	2.9114	0.0621
18	0.3747	0.2759	0.3380	0.6582	6.0000	2.8228	12.0000	5.6456	0.0236
19	0.4241	0.6861	0.5000	0.6772	4.7595	1.0506	9.5190	2.1013	0.0225
20	0.4886	0.5038	0.3532	0.6905	4.5823	2.5190	9.1646	5.0380	0.0369
21	0.3880	0.3291	0.4443	0.6259	3.8734	2.1899	7.7468	4.3797	0.0325
22	0.4734	0.4734	0.4038	0.5880	5.1139	3.0000	10.2278	6.0000	0.0326
23	0.4962	0.6709	0.1405	0.5538	3.2089	1.5570	6.4177	3.1139	0.0265
24	0.4222	0.2380	0.1152	0.6924	4.3165	1.6076	8.6329	3.2152	0.0283
25	0.4013	0.4506	0.1304	0.5671	5.9557	1.7342	11.9114	3.4684	0.0221
26	0.4354	0.4127	0.3076	0.6506	5.7342	1.3291	11.4684	2.6582	0.0218
27	0.4658	0.7848	0.1456	0.6734	3.2975	2.4177	6.5949	4.8354	0.0467
28	0.4468	0.4430	0.3278	0.6962	2.5443	2.1646	5.0886	4.3291	0.1881
29	0.3823	0.7316	0.4544	0.5633	4.7152	2.8734	9.4304	5.7468	0.0334
30	0.4772	0.5949	0.4747	0.5728	2.8544	1.7848	5.7089	3.5696	0.0339
31	0.3652	0.6253	0.1608	0.6601	5.4684	2.0633	10.9367	4.1266	0.0213
32	0.3994	0.5114	0.3228	0.5519	3.9620	1.2532	7.9241	2.5063	0.0236
33	0.4563	0.6405	0.3886	0.6791	5.7785	1.6835	11.5570	3.3671	0.0238
34	0.3918	0.2684	0.3127	0.5500	4.9810	1.7595	9.9620	3.5190	0.0217
35	0.3937	0.3671	0.1861	0.5766	4.4494	1.0000	8.8987	2.0000	0.0212
36	0.4203	0.6481	0.3025	0.6658	4.4937	2.3924	8.9873	4.7848	0.0300
37	0.3595	0.5873	0.2772	0.6487	3.6519	1.0253	7.3038	2.0506	0.0229
38	0.3633	0.3595	0.4797	0.5614	3.8291	1.4304	7.6582	2.8608	0.0270
39	0.4639	0.7013	0.2570	0.5652	3.7405	2.2658	7.4810	4.5316	0.0301
40	0.3614	0.7696	0.2418	0.5842	3.4304	2.6962	6.8608	5.3924	0.0344
41	0.4525	0.3519	0.3684	0.5785	3.6076	1.3797	7.2152	2.7595	0.0239
42	0.4032	0.3367	0.2367	0.6943	4.5380	2.5949	9.0759	5.1899	0.0380
43	0.3899	0.3899	0.2316	0.6203	5.2911	2.2152	10.5823	4.4304	0.0251
44	0.4696	0.2532	0.1000	0.5937	4.1392	1.1013	8.2785	2.2025	0.0201
45	0.4848	0.5190	0.1051	0.6032	2.9430	2.4937	5.8861	4.9873	0.0611
46	0.4316	0.7544	0.3785	0.5709	4.8038	1.7089	9.6076	3.4177	0.0232
47	0.4829	0.5418	0.1557	0.6525	2.5886	1.3038	5.1772	2.6076	0.0395
48	0.4089	0.4658	0.4291	0.6696	4.0063	1.5063	8.0127	3.0127	0.0274
49	0.4373	0.2608	0.2671	0.6639	2.7658	2.6203	5.5316	5.2405	0.1188

50	0.4335	0.5797	0.2620	0.6886	4.2722	1.2278	8.5443	2.4557	0.0231
51	0.4620	0.3747	0.1253	0.5994	4.4051	2.8481	8.8101	5.6962	0.0324
52	0.3861	0.7924	0.2823	0.6563	5.9114	2.6456	11.8228	5.2911	0.0267
53	0.4791	0.5646	0.4241	0.6070	4.9367	1.1772	9.8734	2.3544	0.0217
54	0.3519	0.7089	0.3481	0.6848	3.9177	2.5696	7.8354	5.1392	0.0510
55	0.4070	0.4051	0.2266	0.5557	3.3418	2.0127	6.6835	4.0253	0.0297
56	0.4108	0.6177	0.3937	0.6867	2.5000	2.9494	5.0000	5.8987	0.1360
57	0.3709	0.4962	0.1203	0.6335	4.6709	1.1519	9.3418	2.3038	0.0214
58	0.4867	0.7392	0.1810	0.6715	5.8228	2.7468	11.6456	5.4937	0.0222
59	0.4810	0.2228	0.4494	0.5899	4.0506	1.8101	8.1013	3.6203	0.0274
60	0.4392	0.6937	0.4139	0.6753	2.9873	1.9873	5.9747	3.9747	0.0472
61	0.4297	0.2152	0.2519	0.6278	3.6962	1.2785	7.3924	2.5570	0.0238
62	0.3956	0.5722	0.4949	0.5861	2.6772	2.7722	5.3544	5.5443	0.0545
63	0.4487	0.2987	0.1962	0.6051	5.3797	1.4810	10.7595	2.9620	0.0222
64	0.3500	0.6785	0.4696	0.6468	5.5127	2.6709	11.0253	5.3418	0.0308
65	0.4582	0.4203	0.2975	0.5823	2.7215	2.3165	5.4430	4.6329	0.0466
66	0.3766	0.3823	0.2165	0.5804	4.2278	2.9747	8.4557	5.9494	0.0333
67	0.4051	0.2304	0.3987	0.7000	5.4241	2.2405	10.8481	4.4810	0.0299
68	0.4601	0.6633	0.2215	0.5576	5.6013	1.6582	11.2025	3.3165	0.0212
69	0.3690	0.2076	0.2873	0.6544	4.6266	1.9114	9.2532	3.8228	0.0274
70	0.4411	0.6329	0.4595	0.6165	5.0696	2.1139	10.1392	4.2278	0.0273
71	0.3538	0.4810	0.4342	0.6127	4.8924	1.8354	9.7848	3.6709	0.0283
72	0.4506	0.7772	0.3329	0.6430	3.5633	1.5316	7.1266	3.0633	0.0251
73	0.4544	0.6025	0.1506	0.6108	4.3608	1.8608	8.7215	3.7215	0.0244
74	0.4449	0.3215	0.3835	0.6297	5.2025	2.4430	10.4051	4.8861	0.0276
75	0.4981	0.7620	0.1759	0.6620	4.1835	1.3544	8.3671	2.7089	0.0229
76	0.5000	0.8000	0.4646	0.6184	3.2532	2.3418	6.5063	4.6835	0.0407
77	0.3975	0.6557	0.1101	0.6089	3.1646	2.1392	6.3291	4.2785	0.0328
78	0.3671	0.3063	0.4848	0.6677	2.6329	1.2025	5.2658	2.4051	0.0377
79	0.4943	0.4354	0.2924	0.5918	5.6899	1.9620	11.3797	3.9241	0.0232
80	0.3804	0.2911	0.1658	0.6373	3.0316	1.5823	6.0633	3.1646	0.0340
81	0.4324	0.4380	0.2229	0.6244	3.4933	2.4253	6.9865	4.8506	0.0360
82	0.4399	0.3939	0.1801	0.5913	2.9888	1.5324	5.9777	3.0647	0.0268
83	0.3803	0.2877	0.1656	0.5832	4.9817	2.6788	9.9634	5.3575	0.0270
84	0.4283	0.4398	0.1407	0.5854	4.6427	2.6263	9.2853	5.2527	0.0274
85	0.3882	0.3432	0.4361	0.5940	4.9206	1.5172	9.8412	3.0343	0.0241

86	0.4327	0.4799	0.3873	0.5695	3.9093	2.6660	7.8185	5.3321	0.0372
87	0.4764	0.6067	0.4734	0.6573	3.6181	1.9742	7.2363	3.9485	0.0398
88	0.3592	0.4912	0.1137	0.5681	4.7283	2.1038	9.4566	4.2075	0.0243
89	0.4970	0.4999	0.3136	0.6974	3.9827	2.4128	7.9654	4.8256	0.0429
90	0.3766	0.7733	0.4966	0.5583	5.9979	2.1839	11.9957	4.3678	0.0267
91	0.3671	0.6002	0.2757	0.6922	4.5935	1.4378	9.1870	2.8757	0.0243
92	0.3775	0.5611	0.3248	0.6203	2.9015	2.8536	5.8030	5.7071	0.0467
93	0.3821	0.2419	0.2980	0.6714	4.3319	1.9434	8.6637	3.8867	0.0305
94	0.4134	0.4199	0.2165	0.6894	5.6585	1.2889	11.3170	2.5778	0.0218
95	0.3772	0.4771	0.4101	0.6232	4.9994	1.2516	9.9987	2.5033	0.0228
96	0.4520	0.5216	0.4550	0.5582	3.1649	1.7415	6.3299	3.4829	0.0313
97	0.3825	0.4297	0.2383	0.6921	3.9291	1.8110	7.8582	3.6219	0.0320
98	0.3909	0.6868	0.1798	0.6648	5.8676	1.5191	11.7352	3.0383	0.0218
99	0.4117	0.2782	0.1943	0.6931	3.8984	2.6044	7.7969	5.2087	0.0462
101	0.3801	0.6152	0.4184	0.6991	4.4027	2.0802	8.8054	4.1604	0.0328
102	0.3695	0.2674	0.1827	0.6589	3.0965	1.2895	6.1929	2.5790	0.0347
103	0.3537	0.7474	0.2229	0.6777	3.8372	2.0358	7.6745	4.0716	0.0312
106	0.4118	0.2089	0.3879	0.6965	3.3641	1.4594	6.7281	2.9189	0.0337
107	0.4949	0.5536	0.1635	0.5928	5.7676	2.8232	11.5352	5.6464	0.0281
108	0.4836	0.2742	0.3118	0.5789	4.1264	2.9618	8.2528	5.9236	0.0362
109	0.4612	0.4368	0.1533	0.6963	5.4999	1.8491	10.9997	3.6982	0.0255
110	0.4999	0.3213	0.4538	0.6653	5.2262	1.3646	10.4524	2.7291	0.0239
111	0.3893	0.5012	0.2315	0.6795	5.3100	1.9864	10.6200	3.9727	0.0261
112	0.4129	0.3147	0.4309	0.6740	5.5632	2.4499	11.1264	4.8998	0.0315
113	0.4159	0.7318	0.3410	0.6706	4.0884	2.6963	8.1769	5.3926	0.0366
114	0.3968	0.4297	0.1538	0.6061	4.7180	1.2394	9.4360	2.4788	0.0223
115	0.4233	0.4805	0.3178	0.6067	3.3902	2.0914	6.7803	4.1828	0.0328
116	0.3500	0.2000	0.1000	0.5500	2.5000	1.0000	5.0000	2.0000	0.0247
117	0.5000	0.8000	0.5000	0.7000	6.0000	3.0000	12.0000	6.0000	0.0318
118	0.4419	0.6829	0.3168	0.6458	4.6679	1.3136	9.3359	2.6272	0.0230
119	0.4177	0.6113	0.2839	0.6334	4.8518	1.4486	9.7035	2.8972	0.0235
120	0.4223	0.7236	0.3210	0.6356	5.1026	1.1472	10.2053	2.2944	0.0225
122	0.3968	0.4162	0.3706	0.5557	4.1611	1.4748	8.3222	2.9495	0.0252
123	0.4449	0.6333	0.3722	0.6644	4.6814	1.7791	9.3628	3.5581	0.0263
124	0.4138	0.5569	0.2076	0.6857	4.8271	2.4224	9.6542	4.8448	0.0303
125	0.3822	0.4365	0.3058	0.6729	5.0409	1.4091	10.0818	2.8181	0.0234

126	0.3904	0.2947	0.3587	0.6661	4.1526	1.7005	8.3052	3.4010	0.0289
127	0.4488	0.6233	0.3052	0.6336	4.3660	2.4031	8.7321	4.8063	0.0301

References

Alam, M. I., 2016, "Multidisciplinary design optimization of stratospheric airship," in *International Council of the Aeronautical Sciences (ICAS 2016)*

Alam, M. I., 2017, "Multi-objective multidisciplinary design optimization of high altitude airships,"

Alam, M. I., Subhani, S., and Pant, R. S., 2014, "Multidisciplinary shape optimization of stratospheric airships," in *International Conference on Theoretical, Applied, Computational and Experimental Mechanics (ICTACEM-2014)*

Ceruti, A., Voloshin, V., and Marzocca, P., 2013, "Multi-Disciplinary Design Optimization of Unconventional Airship Configurations with Heuristic Algorithms," *54th AIAA/ASME/ASCE/AHS/ASC Structures, Structural Dynamics, and Materials Conference* **51**, 1–20.

Cheeseman, I., Aerodynamics, Chapter-02, Khoury, G. A., and Gillett, J. D., 1999, "Airship technology," (Cambridge Aerospace Series: 10, Cambridge University Press, ISBN: 0 521 430 747).

Cheeseman, I., 2012, "Airship technology," Chap. 2:Aerodynamics (Cambridge University Press). pp. 29–30.

Chen, Q., Zhu, M., and Sun, K., 2010, "Analysis to Effects on Conceptual Parameters of Stratospheric Airship with Specified Factors," *Journal of Computers* **6**, 1055–1062.

Chen, S., Cowan, C. F., and Grant, P. M., 1991, "Orthogonal least squares learning algorithm for radial basis function networks," *IEEE Transactions on neural networks* **2**, 302–309.

Forrester, A. I., and Keane, A. J., 2009, "Recent advances in surrogate-based optimization," *Progress in Aerospace Sciences* **45**, 50–79.

Gertler, M., Jan. 1950, "Resistance Experiments on a Systematic Series of Streamlined Bodies of Revolution For Application to the Design of High-Speed Submarines," in *David Taylor Model Basin* (Washington DC).

Ghani, O. A., 2013, "Design optimization of aerodynamic drag at the rear of generic passenger cars using nurbs representation," , 30 – 36.

Gupta, S., and Malik, S., 2002, "Envelope details for demo airship," *Aerial Delivery Research and Development Establishment (ADRDE), Agra*

Jasak, H., 2009, "Openfoam: open source cfd in research and industry," *International Journal of Naval Architecture and Ocean Engineering* **1**, 89–94.

Jekabsons, G., 2009, " RBF: Radial Basis Function interpolation for MATLAB/OCTAVE, Riga Technical University, Latvia, version 1.1 ed.,,"

Kale, S. S., Joshi, P., and Pant, R. R., 2005, "A generic methodology for determination of drag coefficient of an aerostat envelope using CFD," *AIAA 5th ATIO and16th Lighter-Than-Air Sys Tech. and Balloon Systems Conferences*, 1–16.

Kanikdale, T., Marathe, A., and Pant, R., 2004, "Multi-disciplinary optimization of airship envelope shape," in *10th AIAA/ISSMO Multidisciplinary Analysis and Optimization Conference*, p. 4411.

Liu, P., Fu, G.-y. Y., Zhu, L.-j. J., and Wang, X.-l. L., 2013 sep, "Aerodynamic characteristics of airship Zhiyuan-1," *Journal of Shanghai Jiaotong University (Science)*, 679–687.

Lophaven, S. N., Nielsen, H. B., and Søndergaard, J., 2002, *DACE: a Matlab kriging toolbox*, Vol. 2 (Citeseer).

Luo, J., and Lu, W., 2014, "Comparison of surrogate models with different methods in groundwater remediation process," *Journal of earth system science* **123**, 1579–1589.

Matheron, G., 1963, "Principles of geostatistics," *Economic geology* **58**, 1246–1266.

Narayana, C. L., and Srilatha, K. R., July 2000, "Analysis of aerostat configurations by panel methods," in *BLISS Project Document CF 0010* (National Aerospace Laboratories, Bangalore, India).

OnlineResource, 1999, "Basic genetic algorithm,"

OnlineResource, 2004, "Write stl file from surface data,"

OnlineResource, 2007, "Stratellites,"

OnlineResource, 2017, "Openfoam v5 user guide: 5.4 mesh generation with snappyhexmesh,"

Queipo, N. V., Haftka, R. T., Shyy, W., Goel, T., Vaidyanathan, R., and Tucker, P. K., 2005, "Surrogate-based analysis and optimization," *Progress in aerospace sciences* **41**, 1–28.

Ram, C. V., and Pant, R. S., 2010 may, "Multidisciplinary Shape Optimization of Aerostat Envelopes," *Journal of Aircraft* **47**, 1073–1076.

KEY: Ram2010
ANNOTATION: From Duplicate 2 (Multidisciplinary Shape Optimization of Aerostat Envelopes - Ram, C. Vijay; Pant, Rajkumar S.) [1] C. V. Ram and R. S. Pant, Multidisciplinary Shape Optimization of Aerostat Envelopes, J. Aircr., vol. 47, no 3 pp 1073 1076, May 2010.

Sacks, J., Welch, W. J., Mitchell, T. J., and Wynn, H. P., 1989, "Design and analysis of computer experiments," *Statistical science*, 409–423.

Shen, W., Guo, X., Wu, C., and Wu, D., 2011, "Forecasting stock indices using radial basis function neural networks optimized by artificial fish swarm algorithm," *Knowledge-Based Systems* **24**, 378–385.

Suman, S., Lakshmipathy, S., and Pant, R., 2011, "Evaluation of the assumed-transition-point criterion in context of RANS simulations around Lighter-Than-Air vehicles," , 1–10.

Viana, F. A. C., 2011, "SURROGATES Toolbox User ' s Guide," , 0–27.

Viana, F. A., Simpson, T. W., Balabanov, V., and Toropov, V., 2014, "Metamodeling in multidisciplinary design optimization: How far have we really come?." *AIAA JOURNAL* **52**

Wang, Q., Chen, J., Fu, G., and Duan, D., 2009 Nov., "An Approach for Shape Optimization of Stratosphere Airships based on Multidisciplinary Design Optimization," *Journal of Zhejiang University SCIENCE A* **10**, 1609–1616.

Wang, X.-L., Fu, G.-Y., Duan, D.-P., and Shan, X.-X., 2010 jul, "Experimental Investigations on Aerodynamic Characteristics of the ZHIYUAN-1 Airship," *Journal of Aircraft* **47**, 1463–1468.